UCSD-SP 68-1

NASw-56
*
NSG-318

Gamma-Ray Production By Cosmic Rays Observed on OSO-1

Laurence E. Peterson

University of Minnesota, Minneapolis, Minnesota

and

University of California, San Diego

La Jolla, California

July 1967

Gamma-Ray Production by Cosmic Rays Observed on OSO-1

Laurence E. Peterson
University of Minnesota, Minneapolis, Minnesota
and
University of California, San Diego
La Jolla, California

ABSTRACT

The OSO-1, which carried a combination of scintillation counters designed to explore the possibility of cosmic photons, has provided new data on cosmic-ray produced γ-rays. The detectors consisted of a NaI scintillator with a lead collimating shield in the 50-150 kev range and a NaI phoswich type scintillation counter with isotropic response and nominal differential channels of 0.33 to 1.0 kev and 1.0 to 3.0 Mev, respectively. A low-efficiency directional detector over the 0.33-1.0 and 1.0-3.0 Mev range was formed by connecting a third scintillation counter in coincidence with the phoswich counter to form a Compton telescope. In addition to the γ-ray channels, integral and total coincidence counting rates were monitored. Although only about 1 gm/cm^2 matter was forward of the instruments, the counters themselves were buried in 13 kg of local instrument matter and located about 40 cm from the center of gravity of the total 200 kg satellite. The satellite, in a 550 km, 33° inclination circular orbit, covered a magnetic Invariant latitude range of $\Lambda = \pm 45$. Most of the counting rates in orbit were due to cosmic-ray produced γ-rays, as determined from the observation

of a large latitude effect. A series of balloon flights with an identical instrument has allowed an extrapolation of atmospheric γ-rays to the satellite altitude and a determination of the effects of local condensed materials. About 20% of the 1 Mev flux of 0.8 counts/cm^2-sec-Mev at 8 gms/cm^2 over Yuma, Arizona ($\Lambda = 40^\circ$) is due to production in the 14 kg of instrument mass. At 550 km, $\Lambda = 42^\circ$, the flux at 1 Mev due to the total spacecraft matter is determined to be about 0.5 counts/cm^2-sec-Mev with a differential power law index of 1.55 over the 0.3 - 3.0 Mev range. This spectrum and flux is in reasonable agreement with the production determined on the Ranger III spacecraft in cislunar space, after correction for the diffuse cosmic flux, which contributes about 0.18 counts/cm^2-sec-Mev at 1 Mev. The cosmic-ray produced background flux is a factor of 2.5 less at $\Lambda = 10^\circ$ than $\Lambda = 42^\circ$. About 95% of the flux measured by the 50-150 kev telescope was due to production in the Pb collimator, apparently not all of it due to cosmic-ray effects. Most of the Compton telescope coincidence events are determined to be a background phenomena. The total integral rates of the isotropic detector > 1 Mev are accounted for in terms of the measured photon fluxes, plus known cosmic-ray particle fluxes. The latitude effects and spectral slopes do not permit unambiguous determination of the mechanism for γ-ray production by cosmic rays. Possibilities include secondaries resulting from π° meson decays and γ-rays from neutron capture and inelastic scattering.

Introduction

The availability of rockets and satellites over the past decade has permitted the explorations of regions of space and observation of phenomena unattainable to previous investigators. As a consequence many new scientific discoveries have occurred. Magnetically trapped radiation, which was essentially unpredicted, has now been considerably explored. Magnetic fields at the interplanetary-earth interface are now fairly well understood. New regions of the astronomical electromagnetic spectrum are now being investigated. Since the discovery of cosmic sources radiating in the 1-100 kev range, rocket and balloon X-ray astronomy has become a most powerful field of modern astrophysics. All these new phenomena are characterized by relatively large effects so that exploration has proceeded by simple extension of existing techniques. In contrast, however, attempts to explore the γ-ray range, where predictions had been made of detectable fluxes at 1 and 100 Mev (Morrison, 1958) have failed. Here the intensities have proved weaker and the signal-to-noise problems more severe than initially estimated. In this paper we wish to discuss an exploratory experiment to search for cosmic γ-rays in the 1 Mev range and in particular the physical origin of the various background phenomena which were observed.

The instrument, known as the University of Minnesota Gamma-ray Experiment, was carried on the first Orbiting Solar Observatory (OSO-1). The device consisted of an array of scintillation counters in various shielding and coincidence configurations operating over the nominal range of 50 kev to 3 Mev. The satellite was launched into a 33° inclined, 550 km nearly circular orbit in March 1962. The instrument therefore counted solar and cosmic fluxes, earth albedo and spacecraft γ-rays, in addition to direct

and induced effects caused by brief passages through the lower fringes of the inner trapped radiation zone. These phenomena have been discussed previously (Peterson, 1965). Large background γ-ray fluxes prevented definitive detection of cosmic fluxes; the upper limits obtained have already been reported and are consistent with the results of Ranger III (Metzger, et al 1964) over this energy range. The detailed understanding of the remaining background, caused primary and secondary cosmic ray interactions in the top of the atmosphere and the spacecraft itself is the subject of this work. This has required a series of balloon flights with a similar instrument, resolution of the observed latitude effects, and comparison with related cosmic-ray measurements. The results presented here are correlated with γ-ray background data obtained on the Ranger III and Explorer XI spacecraft.

Instrumentation and Operation

The instrumentation, which has been described in detail elsewhere (Peterson and Howard, 1961) (Peterson and Nitardy, 1961), will be briefly reviewed here. The detector and logic diagram is shown in Figure 1. Three detector systems were provided:

1) A 2.54 cm dia. x 1.27 cm long NaI scintillation counter with a collimating lead shield to provide a directional detector in the 50-150 kev energy range.

2) A 5.1 cm dia. x 5.7 cm long NaI crystal inside a 0.3 cm plastic phosphor. This formed a phoswich scintillation counter which had nearly

an isotropic response and detected γ-rays in two energy ranges; which were set nominally at 0.33 to 1.0 Mev and 1.0 to 3.0 Mev.

3) A Compton telescope consisting of a forward scattering NaI counter and the phoswich scintillator in coincidence. By proper energy selection of the event in the forward crystal, this provides a directional detector of low efficiency in the Mev range.

In addition, the total rate of all events greater than 1 Mev of the isotropic counter and the total coincidence rate of the counters forming the Compton telescope was monitored. These two functions presumably formed a cosmic-ray single counter and a cosmic-ray telescope respectively and provided a check on various background effects. The characteristics and geometrical properties of the various detectors are given in Table I.

The instrument itself weighed about 14 kg and was located about 40 cm from the c of g of the 200 kg payload mass. Although an average of only about one gm/cm^2 of Al was located forward of the instruments, the isotropic counter was buried under about 5 gm/cm^2 of aluminum, magnesium and circuit components and was located in close proximity to the lead collimator of the low energy telescope.

The instrument was placed in the rotating wheel member of the OSO-1 satellite, with the telescopes looking radially outward. The wheel axis is constrained to lie within a few degrees of a plane perpendicular to the earth-sun line by a servo control. The instrument therefore sweeps by the sun, across the celestial sphere and the earth below once every wheel rotation. The nominal wheel period was two seconds. During orbit day a system of photo detectors and sun slits placed around the rim of

the satellite divided the scan into sixteen 22.5 degree sectors, each referenced to the solar direction and identified by a binary sector code. Telescope events were accumulated from the solar direction and one of the 22.5 degree sectors. The sector was advanced each orbit to obtain a complete scan of the sky in the wheel plane about once every day. The isotropic γ-ray events were accumulated continuously.

Information from the various γ-ray channels, after appropriate prescaling, was accumulated in six binary scalers. These counters, together with sync, auxiliary information and the sector code, were dumped non-destructively into a shift register which was read out at about a one bit/sec rate. Nominally, seventy-eight seconds were required to read an entire frame of data onto the telemetry channel. During orbit night, because no solar reference was available, the readout of the binary registers was inhibited. The cosmic-ray single counter and telescope were then scaled, mixed, and read out to the telemetry in a quasi-digital format. Data was accumulated in an onboard tape recorder for about 90 minutes. A command from a Minitrack station caused this data, an entire orbit, to be played back in five minutes. This resulted in an almost continuous data retrieval.

The OSO-1 was launched March 7, 1962, into a circular 550 km orbit with an inclination of 33 degrees and period of 96 minutes. Satellite operation was nearly continuous for 1,038 orbits, after which the onboard tape recorders failed, and data was then obtained only in real time during passes over receiving stations. Still later a failure in the servo system caused additional loss of data. Information was, however, received on an intermittent basis for nearly two years.

Magnetic tapes from the Minitrack network were processed at the Martin-Marietta Corporation, where analog tapes with the composite FM signal and additional timing information were prepared. About 300 complete passes were reduced at Minnesota and converted into a digital format. The remaining passes were played back at the University of California, San Diego using a somewhat more elaborate playback system which was less affected by noise and syncing errors. All the data was merged at UCSD with orbital information supplied by NASA and various additional coordinates were computed.

Gross Interpretation

Inspection of the data indicated the rates of the isotropic counters to be somewhat higher than predicted from a reasonable extrapolation to higher altitudes and lower latitudes of balloon results obtained in preliminary investigations at Minneapolis (Peterson, 1963). A strong magnetic latitude dependence was noted, indicating most of the γ-ray events were due to cosmic-ray effects. During the brief passage through the inner Van Allen zone over the South Atlantic, the rates became exceedingly high, overfilling the accumulating registers. There were no obvious anisotropies in the counting rates of the directional detectors, and their rate was many factors higher than that implied from the isotropic counters. The phoswich counter rates changed slowly with time initially, then stabilized, indicating a change in the effective energy calibration of this detector.

A scintillation counter in a satellite such as the OSO-1 has many possibilities for counting γ-rays, some of which are indicated here:

1. Cosmic or solar γ-rays.

2. Production by cosmic rays in the satellite. These can be due to bremsstrahlung either from the electronic component or interactions resulting from secondary neutrons.

3. Albedo γ-rays produced by cosmic rays in the atmosphere below the satellite.

4. Residual radioactivity in the satellite.

5. Bremsstrahlung from trapped electrons incident on the satellite, or the atmosphere below.

6. Gamma rays from nuclear reactions of trapped protons.

7. Induced radioactivity in the satellite. This may be due to trapped particles or cosmic-ray neutrons.

8. Gamma rays from nuclear fallout products trapped above about 100,000 feet.

Cosmic ray effects are characterized by a variation with magnetic latitude; extra-terrestrial γ-rays are, of course, latitude independent. Radioactivity in the satellite itself was found to be at a very low level by a background measurement on the launch tower. Direct effects due to the trapped radiation are observed when the satellite is known to be in regions of trapped particles; induced radioactivity is also observed. Radioactive fallout must have contributed only a very small fraction to the total counting rates, as determined from published air sampler activity measurements (Gustafson, 1965).

The cosmic-ray effects can be unfolded by studying counting rates as the satellite moves over the earth's surface. A typical orbit, projected on a geographic map is shown in Figure 2. Isocontours of trapped protons fluxes at 600 km are also shown, as are some of the satellite modes which affect data accumulation. In order to systematically treat latitude effects, the rates of the various channels for about a five-minute interval on each pass were fitted piecewise to a curve. The rate was then interpolated from the fit to various reference geographic meridians, and the latitude computed at which the meridian crossing occurred. In this manner, a counting rate versus latitude curve could be generated from a large number of passes. Figure 3 shows the results of this procedure for the isotropic counter at a geographic meridian of 60°E, over the western Indian Ocean.

The upper branch of each curve is due to 25 minute I^{128} activity induced in the NaI crystal by the trapped protons, as has been reported previously (Peterson, 1965), in detail. In this work we shall use only data points which were obtained at a sufficient duration after a passage through the trapped region so that the I^{128} activity has decayed to an insignificant level. Such points form the lower branch of the curves in Figure 3. Other possible activities have half-lives either very short or very long compared to an orbital period. No slow buildup of radioactive background apparently was observed during the two-month duration of prime data acquisition.

Direct analysis of the satellite data does not allow a rectification of the background into components due to local mass, earth albedo, or cosmic fluxes. In order to ascertain the effects of nearby matter, to investigate

the high rates of the telscope channels, and to obtain added information needed in interpretation of the satellite data, a series of ballon investigations was carried out with a similar instrument.

Balloon Flights

The balloon flights were performed during the summer of 1963 from Yuma, Arizona. At this site the geomagnetic latitude is 40°, and the geographic latitude nearly equal to the orbital inclination. As shown in Figure 2, it therefore became possible to compare data from balloon altitudes with that from a satellite 550 km overhead, although at different times. For these investigations, a spare flight unit, identical in mechanical and electrical configuration to the satellite instrument was flown to 106,000 feet (8 gm/cm^2). A second balloon flight was also made, in which all the instrument materials, including the lead shield were removed. The detectors were then positioned in a Styrofoam block in a geometrical relationship similar to that of the flight instruments. On both flights, provisions were made to orient the detector pointing up, down, and at the horizon, and to monitor certain additional counting rates. The results of the balloon flights are shown in Figure 4 and Table II. No significant anisotropies were observed in the counting rates. Addition of 12 kg of local instrument mass to the bare detectors caused a small increase in the rates of the isotropic counter even at very low altitudes, which increased to about a 20% effect at 8 gm/cm^2. The local instrument matter, at least as determined on the balloon, can account for only a part of the total cosmic-ray produced γ-rays observed in orbit. The effects of the remaining 190 kg of satellite matter were not directly determined.

The effect on the coincidence telescope channels was much larger, as shown in Table II. Here the rates decreased nearly a factor of ten when the instrument matter was removed. If one assumes an isotropic γ-ray distribution, the flux as measured by the Compton telescope should agree with the total as determined from the omnidirectional counters. Stated explicitly,

$$\frac{R_T}{G_T \epsilon_T} = \frac{R_{ISO}}{4\pi G_O \epsilon_O} \quad \text{Photons/cm}^2\text{-sec-ster},$$

where R is the rate, G the geometry factor, and ϵ the efficiency of the telescope and the isotropic counters, assumed to be averaged over the same energy range. The rates obtained on the balloon with the bare detectors allow this equality to maintain within knowledge of the parameters. With the local matter present on the balloon and the OSO-1, however, the fluxes inferred from the telescope rates are about a factor of ten over those obtained with the isotropic counter.

A tentative explanation of the very high background of the coincidence channel is due to energetic secondary cosmic-ray electrons in materials adjacent to the telescope. Such electrons will produce many bremsstrahlung photons simultaneously which may independently be counted by the components of the telescope and produce a coincidence event. Although these events are rare and contribute only a small amount to the total flux, the Compton telescope forward efficiency is also low, and a small background rate soon compares with the genuine telescope event rate. Such spurious events are not "accidentals" in the usual sense, in that

they are not reduced by decreasing the resolving time of the coincidence electronics, but are more analogous to the "side-shower" effect long ago noted in cosmic-ray telescopes. Additional support for this hypothesis is obtained from the total coincidence rate, which was a factor of 12 greater than that accountable for by charged particles, and the lack of anisotropies observed on the OSO-1 flight. Because of this overriding background effect, data from the Compton telescopes has not been analyzed in detail. The lesson for future missions is clear, however. Despite the excellent angular response of these devices, it is essential that no condensed materials be located close to the detectors.

Secondary production in the Pb shield also caused deleterious effects for the 50-150 kev telescope, indicated in Table II. The counting rate of the uncollimated detector was 14 counts/cm^2-sec. If the incident flux is nearly isotropic, addition of a perfect collimator would cause the rate to be reduced a factor of telescope solid angle/4π , or 0.05 in this case. Although the shield is not completely opaque, and some production in it was anticipated, the background reduction was expected to be much larger than the factor of five measured. About 95% of the rate of the low energy telescope must be due to production in the shield. Cosmic X-ray fluxes obtained with this instrument must therefore also be read through a large detector background.

Extrapolation to OSO-1

As indicated previously, the choice of balloon launch site allows a direct comparison of atmospheric γ-ray fluxes with those measured on the

OSO-1, 550 km overhead. The results of this comparison are shown in Figure 5 as a linear extrapolation of the balloon rates to zero depth. Here satellite data obtained during the week of March 7 to 14, 1962, before an appreciable detector gain change occurred, are compared with that on the balloon flight of the complete instrument, 26 June 1963. Changes in the primary cosmic-ray flux over this time interval must have only a very small effect on the γ-rays produced at these low latitudes. The intensity of γ-rays measured on the satellite is only slightly less than that at 8 gm/cm^2; the atmospheric spectrum is steeper, however.

Since these low energy γ-rays are produced isotropically, the rate as a function of depth can be predicted, assuming no cosmic fluxes. Deep in the atmosphere, γ-rays are in equilibrium with secondary cosmic rays. An effect due to the nonestablishment of equilibria and effective solid angle may be expected at a few gm/cm^2. Above the atmosphere the rate should decrease as the earth's solid angle, and as $1/r^2$ at large distances. The solid angle of the earth at 550 km is 1.2π. At 106,000 feet and 1 Mev the effective solid angle due to the atmosphere is about 3.8π, assuming uniform production rate per gram above about 100,000 feet. This would predict a reduction of about three in rates between satellite and balloon observations. Since this factor was not observed, satellite production beyond that determined in the balloon work, cosmic fluxes, or more complicated processes must be involved in the extrapolation.

The spectra determined on the balloon and the early passes of OSO-1 at both $\Lambda = 42^\circ$ and $\Lambda = 10^\circ$ are shown in Figure 6. Approximate slopes of

power law spectral fits are also shown for comparison. The steep atmospheric spectrum is usually explained in terms of the multiple Compton scattering buildup of γ-rays below about 1 Mev. The spectrum at the atmospheric-space interface, where this process does not go to completion, is particularly difficult to estimate. It may, however, explain the flatter slope observed on the satellite. The variation with latitude must be interpreted in terms of cosmic fluxes, or latitude dependent background spectra. All these points will be discussed in later sections.

Integral Spectrum

Understanding the composition of the phoswich counter integral rate is needed in order to interpret the "C. R. Singles" data. In addition to counting γ-rays, this detector measures the energy loss spectrum of all the cosmic ray components, at least with the anticoincidence removed. To separate the various losses on the balloon flights, measurements of the phoswich detector were made of both integral rates and differential rates, with and without the phoswich anticoincidence operating.

Figure 7 shows the differential energy losses over the 0.33 - 1.0 Mev and 1.0 to 3.0 Mev range, with the phoswich operating. Presumably this spectrum is entirely due to γ-rays. Also shown are points on the γ-ray spectrum at lower energy, obtained from the differential rates of the 15-45 kev window of the scattering scintillator, and the 50-150 kev range of the lead pipe telescope counter. Since all the measurements shown here were made with the bare detectors, the spectrum is that of atmospheric γ-rays at 8 gm/cm^2 and $\lambda = 40^{\circ}$. These results are in good agreement with those of Vette (1962) at this same location and depth.

The energy loss spectrum rejected by the phoswich and caused by cosmic rays directly may be estimated from the integral rates. Assuming all the events > 3 Mev are due to cosmic rays isotropic over the upper hemisphere, the flux is 0.25/cm^2-sec-ster, in general agreement with the total particle flux measured at this latitude and altitude (McDonald and Webber, 1959). The area of the counter used was the 33 cm^2 of the NaI only, rather than the 46 cm^2 of the total phoswich, since particles cannot lose 3 Mev in the plastic alone. Under the assumption that all the events are non-interacting, Z = 1 minimum ionizing particles, the energy loss spectrum due to charged particle may be calculated. The result of this calculation is also shown in Figure 7. The maximum energy loss occurs for particles going diagonally through the crystal, a 7.5 cm path which gives 56 Mev. Most probably losses are for events passing through the bulk of the detector. "Edge effects" contribute a flat spectrum of 0.025 events cm^2-sec-Mev extending to the lowest energies. That this calculation has general validity is shown by direct measurements of the energy loss spectrum due to cosmic rays in a similar counter (Peterson and Schwartz, to be published).

Inspection of Figure 7 gives the following conclusions: (1) the differential energy losses in the phoswich counter due to atmospheric γ-rays completely dominate those due to edge effects of cosmic rays over the 0.3 to 3 Mev range. This means that a phoswich type anticoincidence is not required with large crystals operating up to a few Mev in the atmosphere; (2) most of the events rejected by the phoswich, about 20% of the total as shown in Figure 7, must therefore be genuine γ-ray events

rejected because a Compton scattered electron entered the plastic, or due to the operation of the phoswich electronics circuit. From Figures 6 and 7, it may also be shown that the integral counting rate due to photons > 400 kev is about the same as that due to cosmic-rays.

The total integral spectrum can be determined from the results shown in Figures 6 and 7. This is shown in Figure 8, compared with measured points on the balloon flight at 0.33 and 3.0 Mev. The integral rate on the satellite at $\Lambda = 42^{\circ}$ can be also determined using similar considerations, as shown in Figure 8. The point at 1 Mev furnishes the normalization for the particle fluxes; no additional checks are available.

The integral rate obtained at this same location on occasion throughout the satellite lifetime, together with the curves in Figures 8, is used to determine the energy of the "1 Mev" discriminator, and therefore the calibration of the entire phoswich counter. Although this procedure is subject to considerable uncertainties, and is no substitute for a direct calibration, it is estimated the gain is known to about 20%. During the major period of data collection, the phoswich channels were about 0.5 to 1.5 Mev, and 1.5 to 4.5 Mev, respectively. The photon flux determined at $\Lambda = 42^{\circ}$ using this energy calibration is shown in Figure 6. The agreement with data obtained previous to the gain change gives considerable confidence to this indirect calibration procedure.

Latitude Effects

Coordinate System

Unfolding cosmic-ray effects requires a relation between satellite position and cutoff rigidity. Lin, et al (1963) have demonstrated that the parameter L, defined by McIlwain (1961) as a coordinate for trapped particles, can also be applied to cosmic-ray studies. Because of the steepness of the cosmic-ray energy spectrum, most of the particles reaching a particular location are just above magnetic cutoff and, therefore in quasitrapped orbits. Such orbits are appreciably affected by the local magnetic field configuration, which is accounted for in the computation of the L coordinate. Although recent work (Goodwin, private communication) has shown small inconsistencies in cosmic-ray cutoffs derived from L, these effects are neglectable for the purposes of this work.

Using L has the important advantage that it accounts for cut-off rigidity variations as a function of satellite altitude r. The invariant latitude Λ, defined from the relation

$$\Lambda = \cos^{-1} \left(\frac{1}{L}\right)^{\frac{1}{2}},$$

is particularly useful when comparing satellite data with cosmic-ray latitude effects. The relation between Λ, r, and λ has been discussed by McIlwain (1966).

If the earth's field were a pure earth-centered dipole, Λ and the geographic latitude λ would coincide at r = 1. Figure 9 shows Λ, both at the satellite altitude and at the earth's surface as a function of λ at the 60° E geographic meridian, where most of the data presented here has been obtained. The discontinuity occurs because L becomes less than unity;

Λ, therefore, has no meaning. Also shown for comparison is the magnetic latitude λ as obtained from an eccentric dipole model of the geomagnetic field. In this work we have usually assumed the magnetic latitude is equivalent to the invariant latitude at the earth's surface.

Cutoff rigidities can be obtained from L through the relation $R = 14.7/L^2$, as in the case of a pure dipole field (Lin et al, 1963). Although this cutoff may be quite well defined for cosmic rays at the satellite, the rigidity pertinent to cosmic-ray produced γ-rays is not so simple. Atmospheric albedo γ-rays measured on the satellite are obtained from a wide rigidity range. For example, at the 60° E meridian, 550 km and -33°, the cutoff at the satellite is 3.7 BV and is 4.2 BV at the earth's surface directly below. Half of the albedo γ-rays reaching the satellite are collected from a latitude range of $\pm 18^{\circ}$, which corresponds to a cutoff rigidity range of 0.8 to 10.2 BV. Furthermore, the cutoff as defined strictly only applies to the vertical direction and, therefore, neglects east-west effects. These phenomena tend to smooth the γ-ray variation with latitude and cause uncertainties in production functions derived from cosmic-ray cutoffs. For purposes of this work it is assumed that these corrections are of second order, and satellite cutoff rigidities are used. This is particularly valid since most of the background γ-rays apparently result from local production in the satellite.

Cosmic Ray Effects

The counting rates of all the detectors as a function of invariant latitude are plotted in Figure 10. Each point represents a pass crossing the 60° E meridian, derived as explained previously. Data at this meridian has been most extensively studied because many passes can be obtained free

from both local and delayed trapped radiation effects. Here also the L contours are relatively smooth and the balloon site is nearly conjugate in latitude, longitude and Λ. Also shown in Figure 10 are the cutoff rigidities appropriate to Λ.

Integral rates of the isotropic counter show the most pronounced latitude effect. The two photon ranges of this counter indicate the latitude dependent γ-ray spectrum implied by Figure 6. Production in the lead shield is apparently nearly latitude dependent. The total coincidence rate, too large to be explained in terms of direct particle effects, shows a dependence intermediate between the photon and integral channels of the isotropic counter.

The cosmic-ray particle flux can be obtained from the counting rate data, based on the previous analysis of the integral spectrum of the isotropic counter. By correcting the integral rates > 1.5 Mev for the measured photon flux between 1.5 and 4.5 Mev, a rate due mostly to cosmic-ray particles is obtained. To obtain a flux, it is necessary to divide by the isotropic geometry factor, 33 cm^2 and an appropriate solid angle. This must be at least 2.8π, the solid angle subtended by space at 550 km. Here 4π is used, which helps correct for primary and reentry charged albedo, charged secondaries produced in the spacecraft, and γ-rays > 4.5 Mev.

The resultant flux, plotted against cutoff rigidity at the satellite, is shown in Figure 11, compared with various balloon measurements. The total flux data of Winckler, et al (1950) are at 15 gm/cm^2 and those of McDonald and Webber (1959) are for protons only corrected to zero depth. Also shown are Winckler's results as corrected for secondaries by Webber (1958). The

general agreement of the OSO results indicates the interpretation of the isotropic counter integral rate is indeed correct. The discrepancy in absolute value is doubtless due to uncertainties in effective solid angle, cosmic ray anisotropies, spacecraft production, or the correction for higher energy photons.

Gamma-Ray Production

The measured photon fluxes must be due to either extra-terrestrial γ-rays or cosmic-ray produced γ-rays, either resulting from secondary neutron interactions or from degraded products after π^{o} decays. Although each of these components has a unique spectrum and latitude dependence, the rectification cannot be accomplished by interpretation of the data in Figures 6 and 10 alone.

The OSO-1 results have been used previously to provide upper limits on the total cosmic γ-ray flux (Peterson, 1966). These limits are consistent with the measurements in space on Ranger III (Metzger, et al, 1965). Recent evidence has indeed confirmed the Ranger results, thus providing independent knowledge of the cosmic component contributing to the OSO-1 detector rates. The Ranger spectrum compared with the OSO flux at $\lambda = 0$ is shown in Figure 12.

Figure 13 shows the measured photon fluxes, uncorrected for counter efficiency, as a function of Λ. Here we equate Λ with the magnetic latitude at the earth's surface in order to compare with cosmic-ray work. Also shown are the fluxes corrected for the latitude-independent cosmic flux from Figure 12, according to a procedure described in detail previously (Peterson, 1966). Because of the relatively steeper cosmic γ-ray spectrum, the

correction is largest in the lower energy range, and the resultant latitude dependences are nearly identical. We now interpret the "corrected" curves of Figure 13 as being the true latitude function of the cosmic-ray produced γ-rays measured on the OSO-1. The spectrum of these γ-rays is nearly independent of latitude, and slightly flatter than any of the spectra of Figure 6. Because of the reduced effects of multiple Compton scattering, photons in the 1.5-4.5 Mev range probably give a more accurate measure of the production function.

The cosmic-ray proton flux, computed according to an integral energy spectrum $J\ (>E) = \frac{5700}{E1.45}$ (Frier and Waddington, 1965) is also shown in Figure 13. This spectrum fits the points of McDonald shown in Figure 11. The photon latitude dependence is different from that of the primary cosmic-ray flux. Secondary photon production is therefore dependent not only on the number, but the energy of the incident cosmic-ray particles. This is illustrated quantitatively in Figure 14, where the production of 1.5-4.5 Mev photons per cosmic ray particle having rigidity > R has been plotted as a function of R. The "corrected" curve of Figure 13 has been divided by the cosmic-ray proton flux, with the photon flux assumed isotropic over 4π and the γ-ray energy interval taken to be 3 Mev. It is this production curve, and the absolute value of the source strength, which a complete theory of cosmic-ray produced γ-rays must explain.

Lacking such a theory, the latitude dependence may indicate the physical processes operating. Photons originating from π^{o} meson decays should be in equillibrium with secondary cosmic-ray mesons. Shown in Figure 13 is the average integral meson multiplicity for the cosmic-ray spectrum, defined as

$$M(>E) = \frac{1}{N(>E)} \int_{E}^{\infty} \bar{m}(\epsilon) \frac{dN}{d\epsilon} d\epsilon,$$

plotted as a latitude function. The Fermi multiplicity $\bar{m}(\epsilon)$ has been used here and the cosmic-ray spectrum is that of Figure 13. Although this calculation fails to account for the kinematics of the average meson producting interaction, and therefore the detailed energy transport of primary cosmic rays into a γ-ray producing component, the latitude derived effect is nevertheless similar to the experimentally obtained photon production curve. Also shown are the relative values of earth albedo γ-rays in the 100 Mev range determined on the Explorer XI gamma-ray experiment (Kraushaar, et al, 1965). This flux should originate directly from π^{o} decays, its agreement with the calculated latitude effect can hardly be fortuitous.

Gamma rays due to direct nuclear interactions should be proportional to the equilibrium albedo neutron flux. The latitude dependence of this component at solar minimum obtained from the calculations of Lingenfelter, (1963), is also shown in Figure 13. Earlier work by Hess, et al (1961) gives a slightly flatter latitude function. Also shown are the albedo neutron fluxes determined from a series of balloon measurements (Holt, Mendell and Korff, 1966).

Clearly, latitude dependence does not provide unique distinction between the originating mechanisms for secondary γ-rays, at least with the rudimentary data and theory presently available. Other evidence, based on balloon work (Vette, 1962, Peterson, 1963) indicates most of the source is indeed from π^{o} meson decays. The source can best be determined from the

details of the γ-ray spectrum, data which is not provided by the OSO-I experiment, but has been obtained from further work (Peterson and Schwartz, to be published).

Production in Lead

The latitude dependence of the 50-150 kev lead pipe telescope background seems anomolous, when compared with other effects shown in Figures 10 and 13. Furthermore the production in the lead at $\Lambda = 42^{\circ}$, 3.1×10^{-2} photons/gm-sec-kev, seems completely disparate with the value of 1.05×10^{-2} photons/gm-sec-kev reported by Vette (1962) at 6 gm/cm^2 over Yuma. Rather than invoke peculiar latitude and altitude dependent cosmic ray production mechanisms, other effects seem more likely. Preflight calibration data shows that at no time did this telescope have a rate less than about 3 c/sec. indicating a possible low-level radioactive contamination. Another possibility includes production of a several day isotope in the lead by trapped protons. Such activity could not have been found in the data analysis. Because of these uncertainties, latitude dependent cosmic-ray production functions cannot be derived for lead from the OSO-1 data.

Spacecraft Production

The background flux produced in the OSO spacecraft by cosmic-ray phenomena may now be determined. Here we correct the measured fluxes for the extraterrestrial diffuse component, and the fluxes attributed to the earth albedo as inferred from the balloon data. As discussed previously, the latter is the flux measured at 8 gm/cm^2 reduced by the effective solid angle ratio $1.2\pi/3.8\pi$. This assumes that the production rate per gram in the upper 20 gm/cm^2 of

atmosphere is fairly independent of depth. Attenuation in satellite materials shielding the isotropic counter is also neglected. Effects due to non-isotropic absorption of albedo or cosmic γ-rays were not observed, as determined by comparing rates at a given meridian and latitude as the satellite aspect changed.

The spectrum which results from carrying out these procedures is shown in Figure 15 for the satellite at $\Lambda = 42^{\circ}$. Similar results for other latitudes were not determined, because of the lack of balloon data to provide the albedo correction. Based on the balloon flights at Yuma, only about 20% of the observed production can be accounted for in terms of local instrument matter. Most of the production must therefore have occurred in the remaining 190 kg of satellite materials.

Also shown in Figure 15 is the flux produced by Ranger III Spacecraft (Metzger, et al, 1964) in cislunar space, as determined by correcting the inboard data for the cosmic flux detected outbound.[1/] Here, as well as in OSO case, smoothed data are shown since the actual errors are difficult to estimate. Both spacecraft apparently produced a background flux very similar in spectrum and magnitude, despite the somewhat different cosmic-ray environments and spacecraft configurations. A detailed comparison of the Ranger and OSO production data requires an analysis in terms of the local materials and their distribution with respect to the detectors. Such an analysis is beyond the scope of this work. The data clearly shows, however, that cosmic-rays interacting in the spacecraft mass produce a very large γ-ray back-

---

1/ The author is indebted to Dr. A. E. Metzger of the Jet Propulsion Laboratory for providing this previously unpublished data.

ground flux. Reduction of effects due to this background requires anti-coincidence shielding, collimated detectors, experiment booms, etc.

Conclusion

The University of Minnesota γ-ray experiment on the OSO-I has provided data on the omni-directional flux of Mev range γ-rays in a 550 km, 30° inclination orbit. The results, together with auxilliary balloon measurements of atmospheric γ-rays and the Ranger III data in space, allows a resolution of the total counting rate into components due to cosmic fluxes, production in the spacecraft, and earth albedo γ-rays. For example, on the OSO-1, about 0.03 c/cm^2-sec in the 1.5-4.5 Mev range, can be attributed to cosmic γ-rays, or 9% of the total rate of $0.35 c/cm^2$-sec at $\Lambda = 42^{\circ}$. If the extrapolation to the satellite of the balloon flux proceeds simply as the effective solid angle, only 0.14 c/cm^2-sec or 40% of the OSO flux can be accounted for in terms of atmospheric albedo. Therefore about 50% of the measured background at $\Lambda = 42^{\circ}$ over the 1.5-4.5 Mev region must be due to production in the spacecraft itself. Similar numbers may be worked out for other energy ranges and latitudes from the data presented here; the conclusion however is unchanged. Spacecraft production determined here for the OSO is also in close agreement with that measured on the Ranger III, exposed to the full intensity of galactic cosmic rays.

Analysis of the 2.5 to 1 magnetic latitude effect, observed over the range from 0 to 45°, does not permit unique determination of the origin of the secondary γ-rays. The major source, determined from other experiments, is that due to degraded products of π_o meson decay, with neutron capture

and inelastically scattered photons producing only a small fraction of the total flux in the Mev range.

Acknowledgments

In a long and complex project such as the University of Minnesota γ-ray Experiment for the OSO-1, it is impossible to acknowledge the contributions of every person involved. Certain individuals and organizations desire particular merit however.

This work was originally suggested by Dr. J. R. Winckler at Minnesota, under whose auspices the project was carried through the launch and initial data reduction phase. Messrs. Robert Howard, William C. Erikson, Gerald Peterson and John Nitardy were responsible for the instrument design, construction, and checkout, and preliminary balloon investigations. Initial data reduction was accomplished by a semi-computerized system programmed and operated by Robert Goodwin.

Reduction at University of California, San Diego was performed on a system constructed and operated by Paul Brissenden. R. M. Pelling directed hand data readouts, and contributed to many phases of the data analysis. Computer programs were written by Mrs. Mary McLaird and Mr. Louis Huszar, who has been entirely responsible for the final stages of data analysis. Mr. Rod Jerde constructed the balloon gondolas. Flight services at UCSD were provided through General Dynamics/Astronautics.

The OSO project would not have existed, except for the late Dr. John C. Lindsay, Project Scientist, of the Goddard Space Flight Center. The satellite itself was designed, constructed, and integrated in a most

expedient manner by personnel at the Ball Brothers Research Corporation, under the direction of Mr. Fred Dolder, Project Engineer.

This research was supported under NASA contracts NASw-56 at Minnesota, and NsG-318 and NAS5-3122 at La Jolla.

References

Freier, P. S. and C. J. Waddington, The helium nuclei of the primary cosmic radiation as studied over a solar cycle of activity, interpreted in terms of electric field modulation, Space Science Reviews 4, 313-372, 1965.

Gustafson, P. F., Gamma-ray spectroscopy in the upper atmosphere using a balloon borne detector, IEEE Trans. on Nucl. Sci., NS-12, 82-87, 1965.

Hess, W. N., E. H. Canfield, and R. E. Lingenfelter, Cosmic-ray neutron demography, J. Geophys. Research, 66, 665-678, 1961.

Holt, S. S., R. B. Mendell, and S. A. Korff, Fast neutron latitude variations in the atmosphere at solar minimum, J. Geophys. Res. 71, 5109-5116, 1966.

Kraushaar, W., G. W. Clark, G. Garmire, H. Helmken, P. Higbie, and M. Agogino, Explorer XI experiment on cosmic gamma rays, Astrophys. J, 141, 845-863, 1965.

Lin, W. C., D. Venkatesan, and J. A. Van Allen, Latitude survey of cosmic-ray intensity by Explorer 7, October 1959 to February 1961, J. Geophys. Res., 68, 4885-4896, 1963.

Lingenfelter, R. E., cosmic-ray neutron leakage flux, J. Geophys. Res. 68, 5633-5639, 1963.

McDonald, F. B. and W. R. Webber, Proton component of the primary cosmic radiation, Phys. Rev. 115, 194-205, 1959.

McIlwain, C. E., Coordinates for mapping the distribution of magnetically trapped particles, J. Geophys. Res. 66, 3681-3691, 1961.

McIlwain, C. E., Magnetic Coordinates, Radiation Trapped in the Earth's Magnetic Field (McCormac, ed.), 45-61, 1966.

Metzger, A. E., E. C. Anderson, M. A. Van Dilla, J. R. Arnold, Detection of an interstellar flux of gamma-rays, Nature, 204, 4960, 766-767, 1964.

Morrison, P., On-Gamma-Ray Astronomy, Nuovo Cimento, 7, 858-865, 1958.

Peterson, L. E. and R. L. Howard, Gamma-ray astronomy in space in the 50-kev to 3-Mev region, IRE Trans. on Nuc. Sci., NS-8, 4, 21-27, Oct. 1961.

Peterson, L. E. and J. H. Nitardy, A simple circuit for a phoswich scintillation counter, Rev. of Sci. Instr., 32 (12), 1390-1392, 1961.

Peterson, L. E., The 0.5-Mev gamma-ray and the low energy gamma-ray spectrum to 6 grams per square centimeter over Minneapolis, J. Geophys. Res., 68, 4, 979-987, 1963.

Peterson, L. E., Upper limits of the cosmic gamma-ray flux from OSO-1, Space Research VI, 53-66, 1966.

Peterson, L. E., Radioactivity induced in NaI by trapped protons, J. Geophys. Res. 70, 1762-1765, 1965.

Vette, J. I., Low-energy gamma rays produced in air and in lead by cosmic rays, J. Geophys. Res., 67, 1731-1739, 1962.

Winckler, J. R., T. Stix, K. Dwight, and R. Sabin, A directional and latitude survey of cosmic rays at high altitudes, The Physical Review, 79, 656-669, 1950.

Webber, W. R., The charge composition and energy spectra of primary cosmic rays and the energy balance problem, Nuovo Cimento Suppl. 8, 532-545, 1958.

TABLE I

DETECTOR CHARACTERISTICS

U. OF M. S-16 γ- RAY EXPERIMENT

DETECTOR	FUNCTION	GEOMETRY FACTOR			EFF.	SHIELDING
		OMNI.	PT. SOURCE	EXT. SOURCE		
PB PIPE TELESCOPE	50-150 Kev Photons	5.06 cm^2	5.06 cm^2	0.283 cm^2-ster.	~ 1.0	1.2 gm/cm^2 Al 5.0 gm/cm^2 Pb
PHOSWICH ISOTROPIC COUNTER	0.3 - 1.0 Mev 1.0 - 3.0 Mev Photons	33 cm^2	-	-	.75 at .66 Mev .62 at 1.28 Mev	~ 5 gm/cm^2 average
COMPTON TELESCOPE	0.3 - 1.0 Mev 1.0 - 3.0 Mev Photons	-	7.9 cm^2	1.3 cm^2-ster.	0.3×10^{-2} at 1.28 Mev.	0.8 gm/cm^2 Al
COSMIC RAY SINGLES	All events > 1 Mev	46 cm^2	-	-	1.0 for cosmic rays	~ 5 gm/cm^2 average
COSMIC RAY TELESCOPE	All coincident events $\Delta t = 1.5 \times 10^{-6}$ sec	-	-	1.7 cm^2-ster.	1.0 for cosmic rays	0.8 gm/cm^2 Al

TABLE II - COMPARISON OF COUNTING RATES
OSO - 1 DETECTORS
ALL RATES COUNTS/SEC

FUNCTION	BALLOON FLIGHTS 8 gm/cm^2 $\lambda = 40^\circ$ Unit Vertical			OSO-I ORBIT H = 550 km 14 March 1962
	Instrument Matter Present 26 June 1963	Instrument Matter Removed 7 Aug. 1963	$\Lambda = 42^\circ$	$\Lambda = 10^\circ$
50-150 kev Telescope	2.6 ± 1.0	14.3 ± 1.1	7.1± 0.5	5.0± 0.5
0.3 - 1.0 Mev Isotropic	46.6 ± 0.5	34.9 ± 0.1	24.0	12.5
1.0 - 3.0 Mev Isotropic	14.25 ± 0.15	11.6 ± 0.1	12.6	6.2
C. R. Singles (> 1.0 Mev Total)	69.4 ± 1.0	64.0 ± 1.1	64 ± 0.6	19.0
0.3 - 1.0 Telescope	$3.3 \pm 0.24 \times 10^{-2}$	$0.27 \pm 0.15 \times 10^{-2}$		
1.0 - 3.0 Telescope	$1.33 \pm 0.16 \times 10^{-2}$	$0.36 \pm 0.2 \times 10^{-2}$		
C. R. Telescope (Total Coincidences)	2.13 ± 0.27	0.71 ± 0.13	3.6	1.4
> 45 Kev, > 150 Kev > 1.0 Mev (3-Fold Coincidences)	0.40 ± .02	0.069 ± .008		

Figure Captions

Figure 1 Block diagram of an exploratory experiment in gamma-ray astronomy designed for the First Orbiting Solar Observatory (OSO-1). The detectors were designed to measure the directional and omnidirectional fluxes, and to provide a crude energy analysis.

Figure 2 A typical orbit of the OSO-1, projected on a geographic map and showing features of the trapped radiation which affected data interpretation. The satellite was in sunlight for about 60 of the 96 minute orbital period. An entire orbit of data was read out during a 5 minute pass over the Minitrack network.

Figure 3 Counting rates vs. geographic latitude at a typical meridian of longitude show two branches, the upper one being due to radio-activity induced by trapped protons. Cosmic-ray produced γ-ray effects and extraterrestrial upper limits are obtained by interpreting the lower curve.

Figure 4 Effect of 14 kg of local instrument matter on the counting rates of the isotropic phoswich counter, as determined on a series of balloon flights. Removing this instrument material resulted in a much larger change in other γ-ray channels than the 25% decrease shown here.

Figure 5 Extrapolation of the balloon results to zero depth. The OSO-1 data points obtained 550 km directly overhead are also shown. Had there been no spacecraft production, and no cosmic fluxes, the rates would have been about one-third those at 8 $gm/_{cm}2$.

Figure 6 The differential photon spectrum measured at 8 $gm/_{cm}{}^2$ and on the OSO-1 at two magnetic latitudes. The steeper atmospheric spectrum may be explained in terms of multiple Compton scattering buildup; the variation at satellite altitudes requires cosmic-ray produced γ-ray spectra dependent on latitude, extraterrestrial fluxes, or both.

Figure 7 An analysis of all the energy losses in the isotropic counter at balloon altitudes. The photons contributed a steep spectrum, cosmic-rays a flat spectrum which was ordinarily rejected by the phoswich electronics circuit. This peaks at energy losses well above the range of interest in this work.

Figure 8 Total integral rates of the phoswich counter at balloon and satellite altitudes, determined from the data of Figure 7. This rate is measured by the "cosmic-ray singles" function and is used, among other purposes, to energy calibrate the detector.

Figure 9 Magnetic and Invariant latitudes at the 60° E geographic meridian, where much of the data presented here has been obtained. The invariant latitude, a useful cosmic-ray coordinate, is derived from the parameter L of McIlwain.

Figure 10 Counting rates of the OSO-1 detectors at the 60° E meridian. Each point represents a pass, selected to be fre from short-term

radio-activity, timing and other errors. Cosmic and locally produced flux must be unfolded by interpreting these curves.

Figure 11 The cosmic-ray rigidity spectrum obtained from the > 1.5 Mev integral rates by correcting for the 1.5 - 4.5 Mev photon flux, and assuming a solid angle of 4π. This compares well with previous balloon determinations of the fluxes.

Figure 12 The OSO-1 data at $\Lambda = 0$, previously interpreted as providing upper limits on cosmic γ-rays, compared with the Ranger III in space. The Ranger results are now well verified and may be used to correct the OSO-1 data.

Figure 13 OSO-1 fluxes as a function of invariant latitude, before and after correction for the isotropic component of cosmic γ-rays. Also shown are the total primary cosmic ray, and secondary meson and neutron fluxes. The latitude dependence does not uniquely indicate the source of the Mev range γ-rays.

Figure 14 Integral productions of function for γ-rays produced mostly in the spacecraft. The true source function cannot be obtained precisely because of the uncertainty of integrating over the entire spacecraft mass.

Figure 15 Background flux observed on the Ranger spacecraft in space, compared to that in the OSO at 550 km and $\Lambda = 42^{\circ}$. Production in the OSO spacecraft itself must have dominated background due to earth albedo γ-rays.

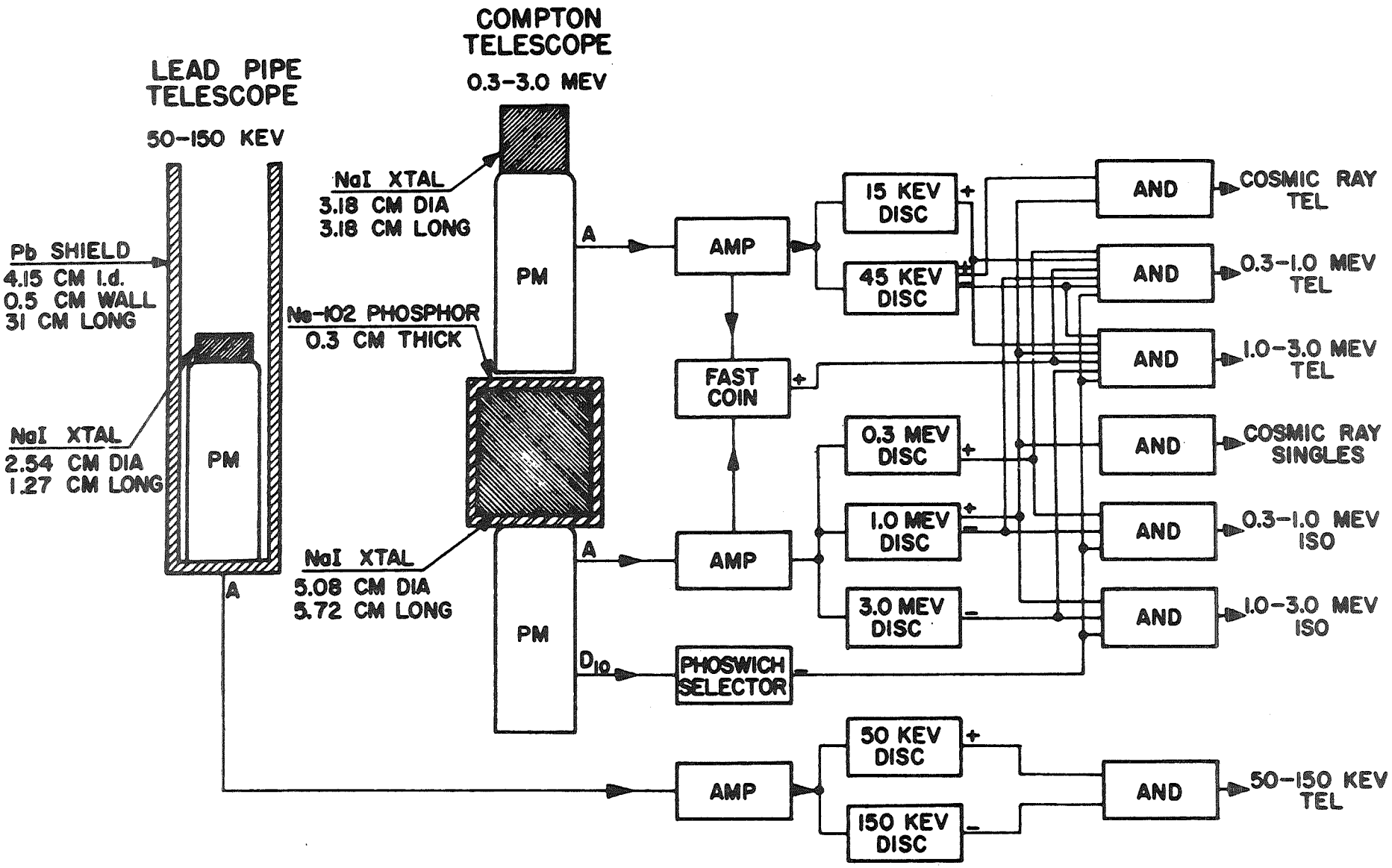

γ-RAY DETECTORS & DETECTOR LOGIC

Figure 1

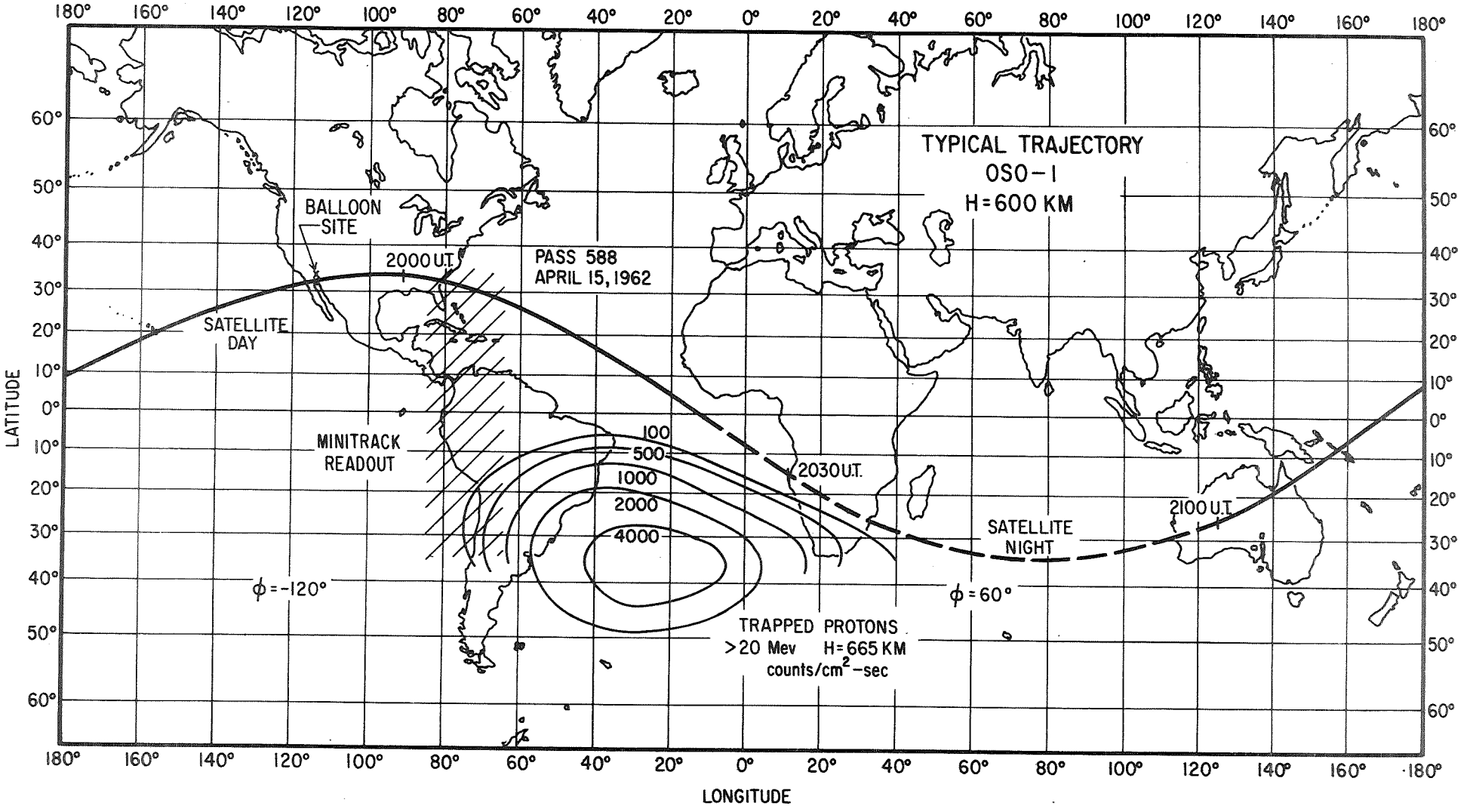
TYPICAL TRAJECTORY
OSO-I
H=600 KM
BALLOON SITE
PASS 588
APRIL 15, 1962
2000 U.T.
SATELLITE DAY
MINITRACK READOUT
100
500
1000
2000
4000
2030 U.T.
2100 U.T.
SATELLITE NIGHT
φ=-120°
φ=60°
TRAPPED PROTONS
>20 Mev H=665 KM
counts/cm²-sec
LATITUDE
LONGITUDE
180° 160° 140° 120° 100° 80° 60° 40° 20° 0° 20° 40° 60° 80° 100° 120° 140° 160° 180°
60° 50° 40° 30° 20° 10° 0° 10° 20° 30° 40° 50° 60°

Figure 2

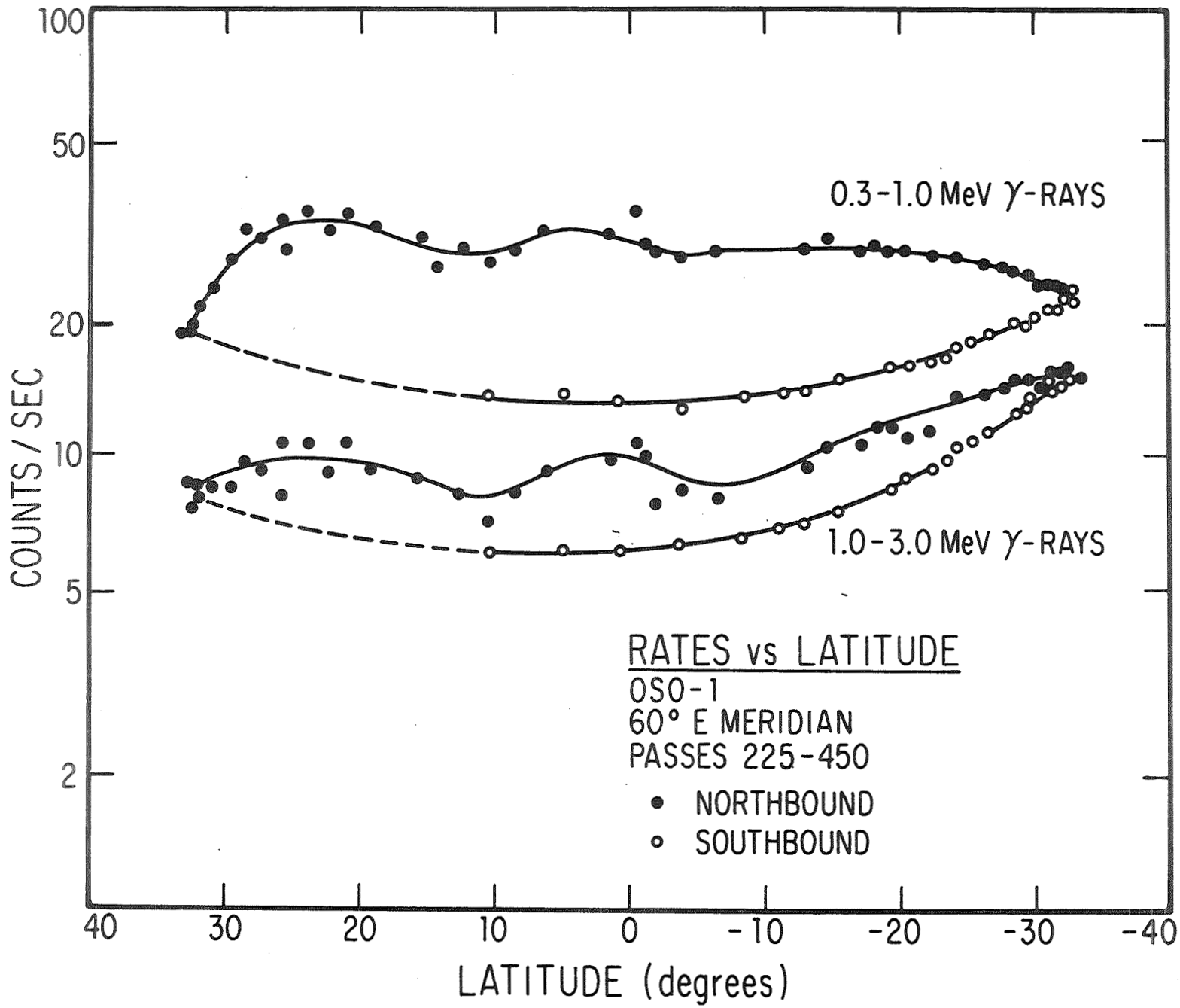
100
50
20
10
5
2
COUNTS / SEC
0.3-1.0 MeV γ-RAYS
1.0-3.0 MeV γ-RAYS
RATES vs LATITUDE
OSO-1
60° E MERIDIAN
PASSES 225-450
NORTHBOUND
SOUTHBOUND
40
30
20
10
0
-10
-20
-30
-40
LATITUDE (degrees)

Figure 3

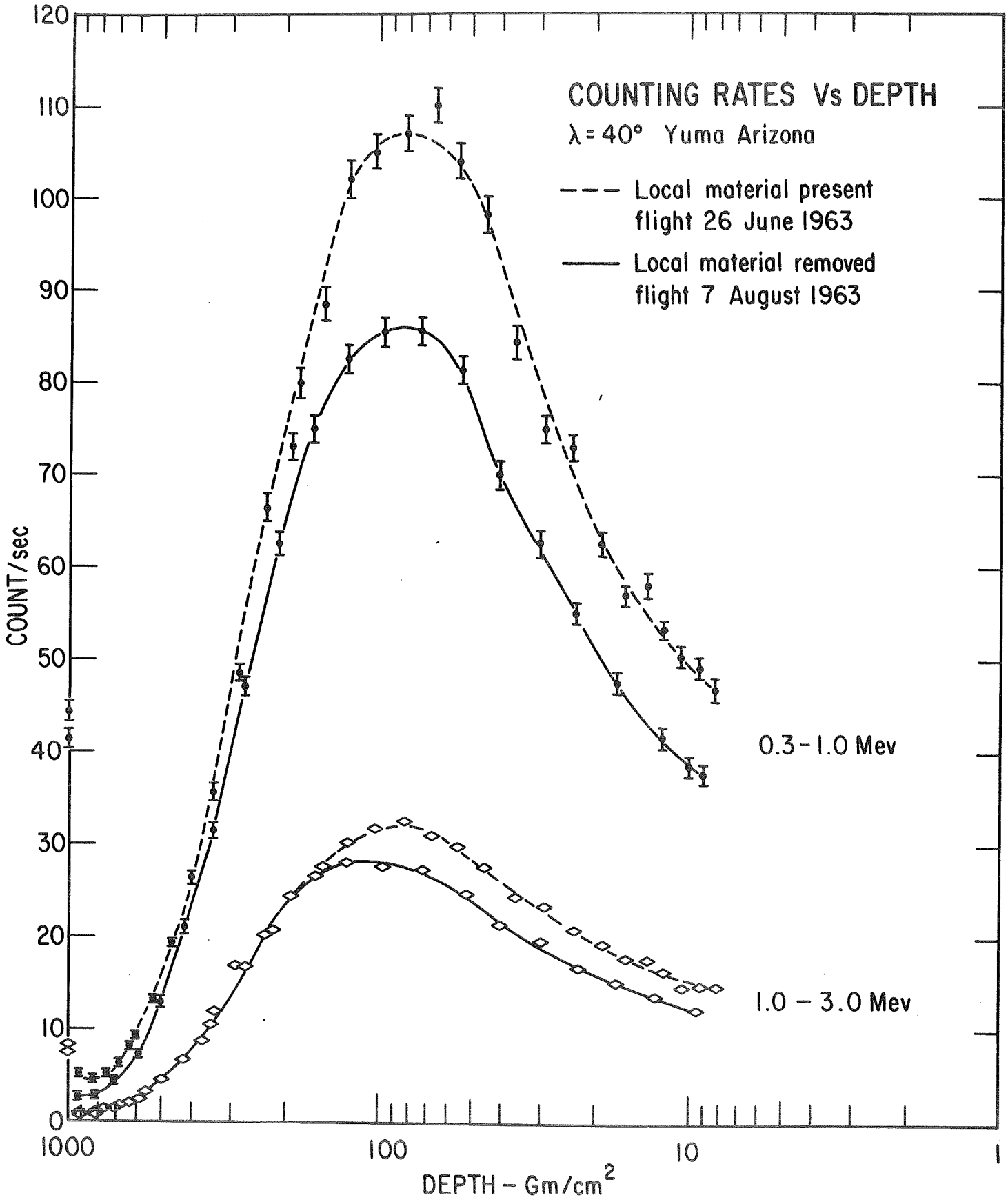
COUNTING RATES Vs DEPTH
λ = 40° Yuma Arizona
Local material present
flight 26 June 1963
Local material removed
flight 7 August 1963
0.3 - 1.0 Mev
1.0 - 3.0 Mev
COUNT/sec
DEPTH - Gm/cm²
120
110
100
90
80
70
60
50
40
30
20
10
0
1000
100
10
1

Figure 4

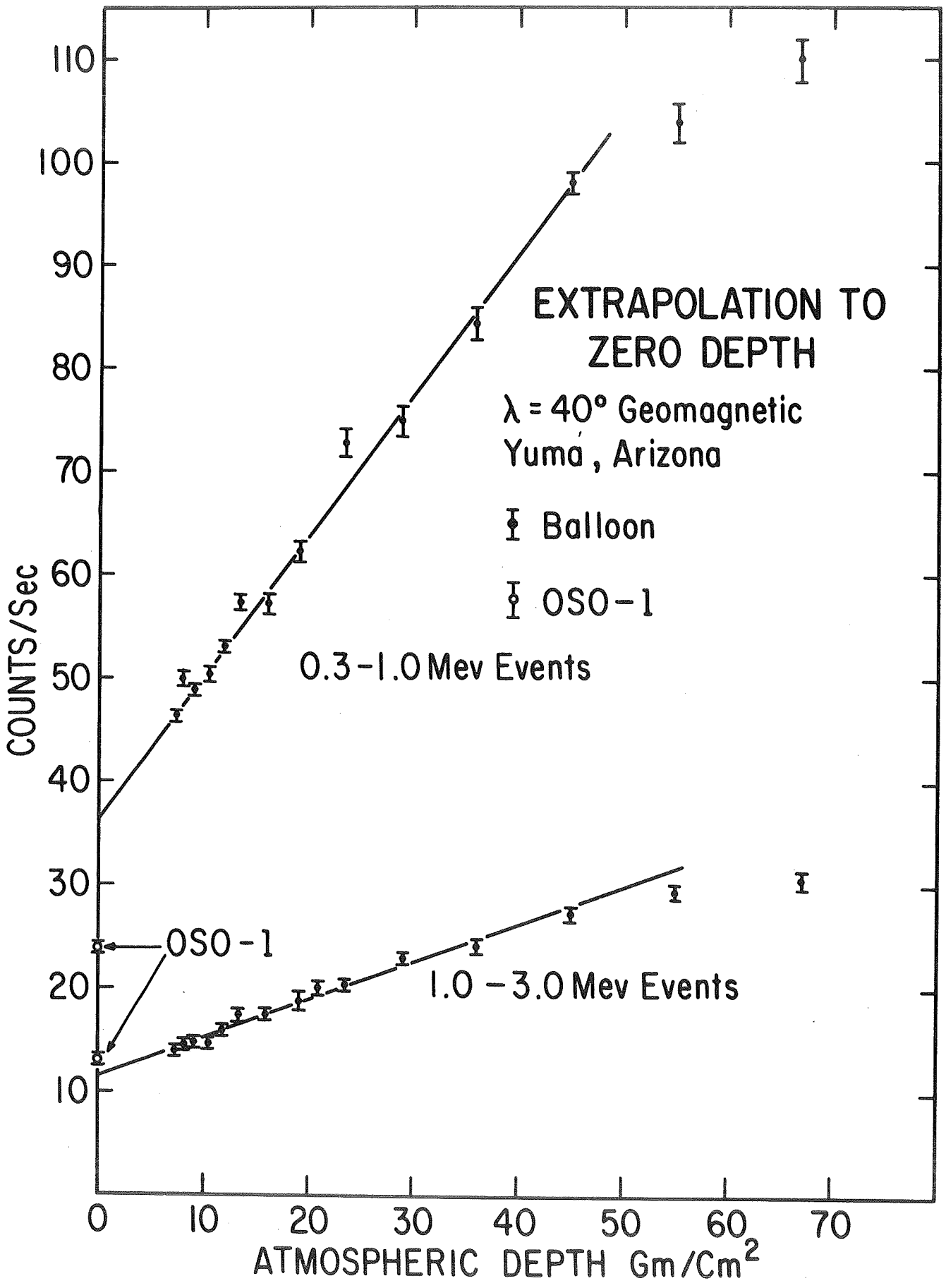
EXTRAPOLATION TO
ZERO DEPTH
λ = 40° Geomagnetic
Yuma, Arizona
Balloon
OSO-1
0.3-1.0 Mev Events
1.0-3.0 Mev Events
OSO-1
COUNTS/Sec
ATMOSPHERIC DEPTH Gm/Cm²
110
100
90
80
70
60
50
40
30
20
10
0
10
20
30
40
50
60
70

Figure 5

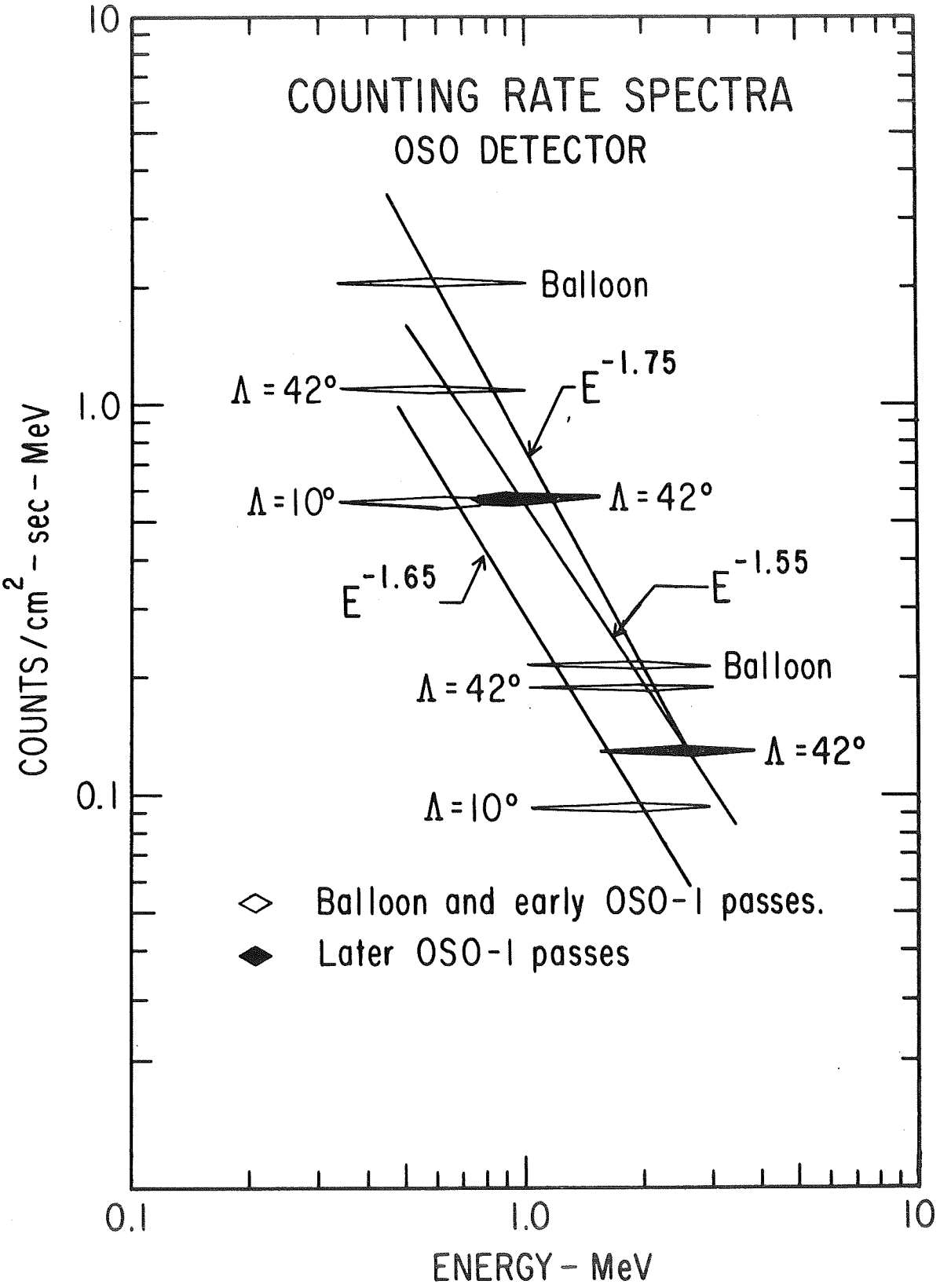
COUNTING RATE SPECTRA
OSO DETECTOR
Balloon
Λ = 42°
E^-1.75
Λ = 10°
Λ = 42°
E^-1.65
E^-1.55
Balloon
Λ = 42°
Λ = 42°
Λ = 10°
Balloon and early OSO-I passes.
Later OSO-I passes
COUNTS/cm^2 - sec - MeV
ENERGY - MeV
10
1.0
0.1
0.1
1.0
10

Figure 6

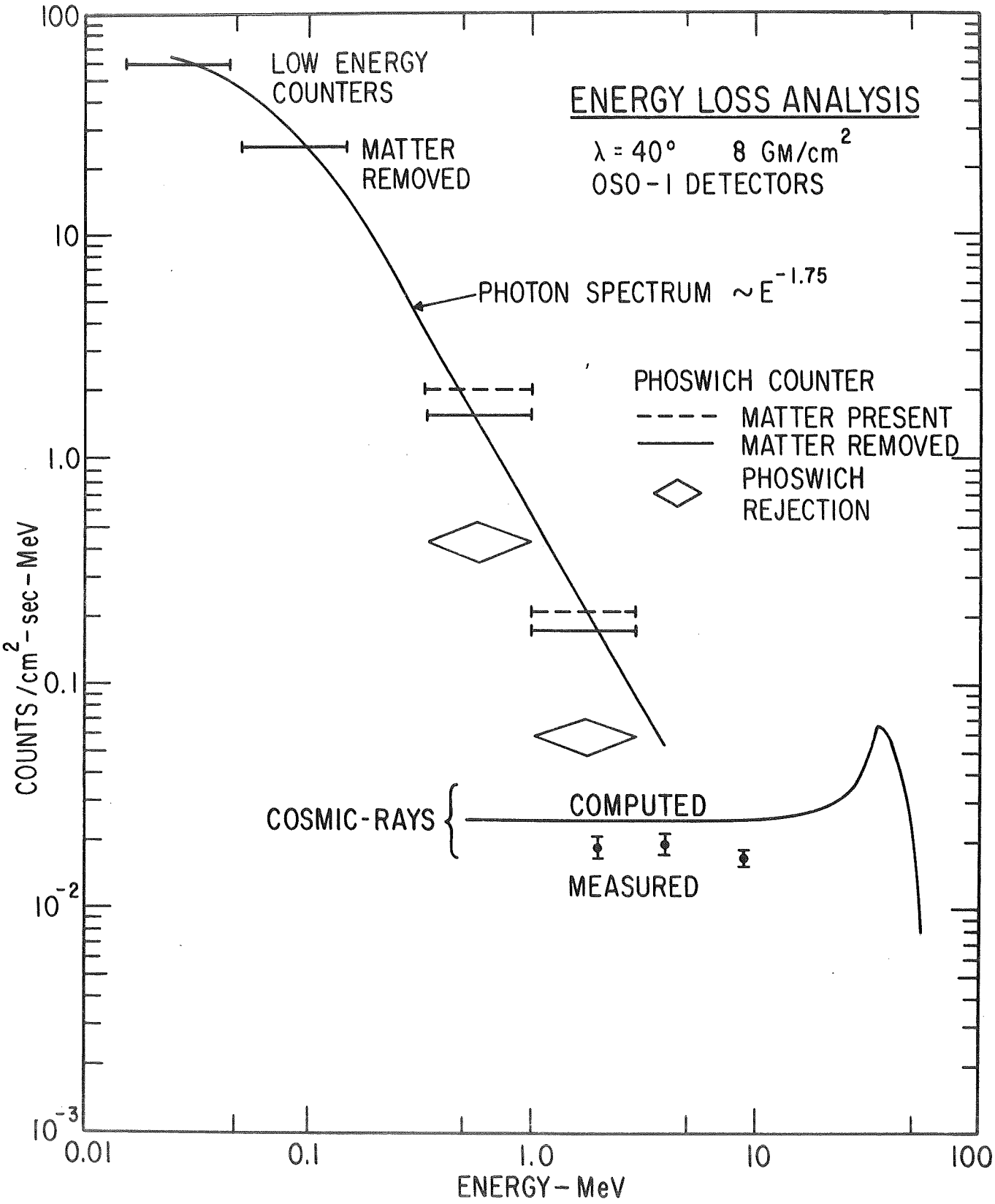
ENERGY LOSS ANALYSIS
λ = 40° 8 GM/cm²
OSO-I DETECTORS
LOW ENERGY COUNTERS
MATTER REMOVED
PHOTON SPECTRUM ~E^-1.75
PHOSWICH COUNTER
MATTER PRESENT
MATTER REMOVED
PHOSWICH REJECTION
COSMIC-RAYS
COMPUTED
MEASURED
COUNTS/cm²-sec-MeV
ENERGY-MeV
100
10
1.0
0.1
10^-2
10^-3
0.01
0.1
1.0
10
100

Figure 7

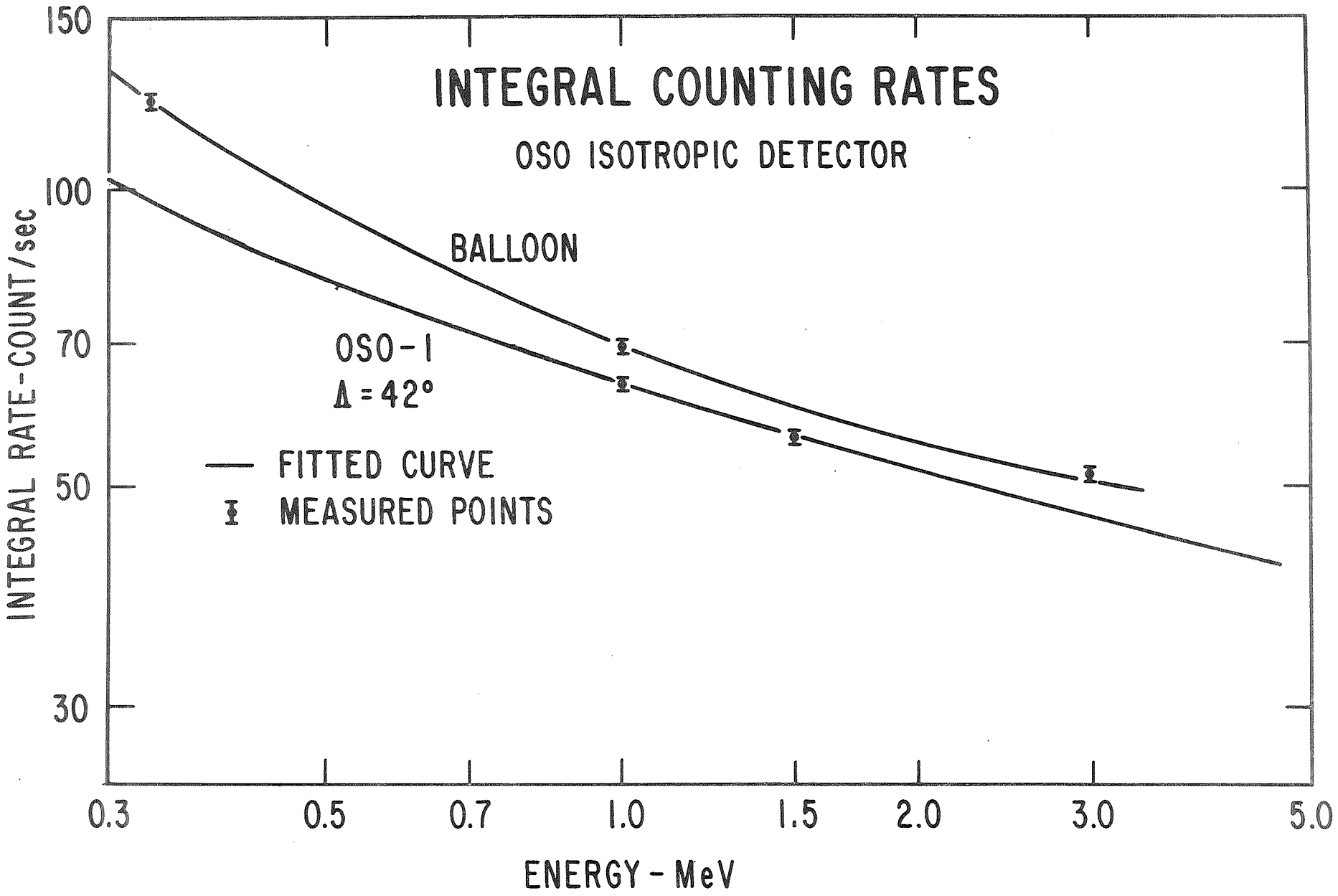
INTEGRAL COUNTING RATES
OSO ISOTROPIC DETECTOR
BALLOON
OSO-I
Λ = 42°
FITTED CURVE
MEASURED POINTS
INTEGRAL RATE-COUNT/sec
150
100
70
50
30
0.3
0.5
0.7
1.0
1.5
2.0
3.0
5.0
ENERGY - MeV

Figure 8

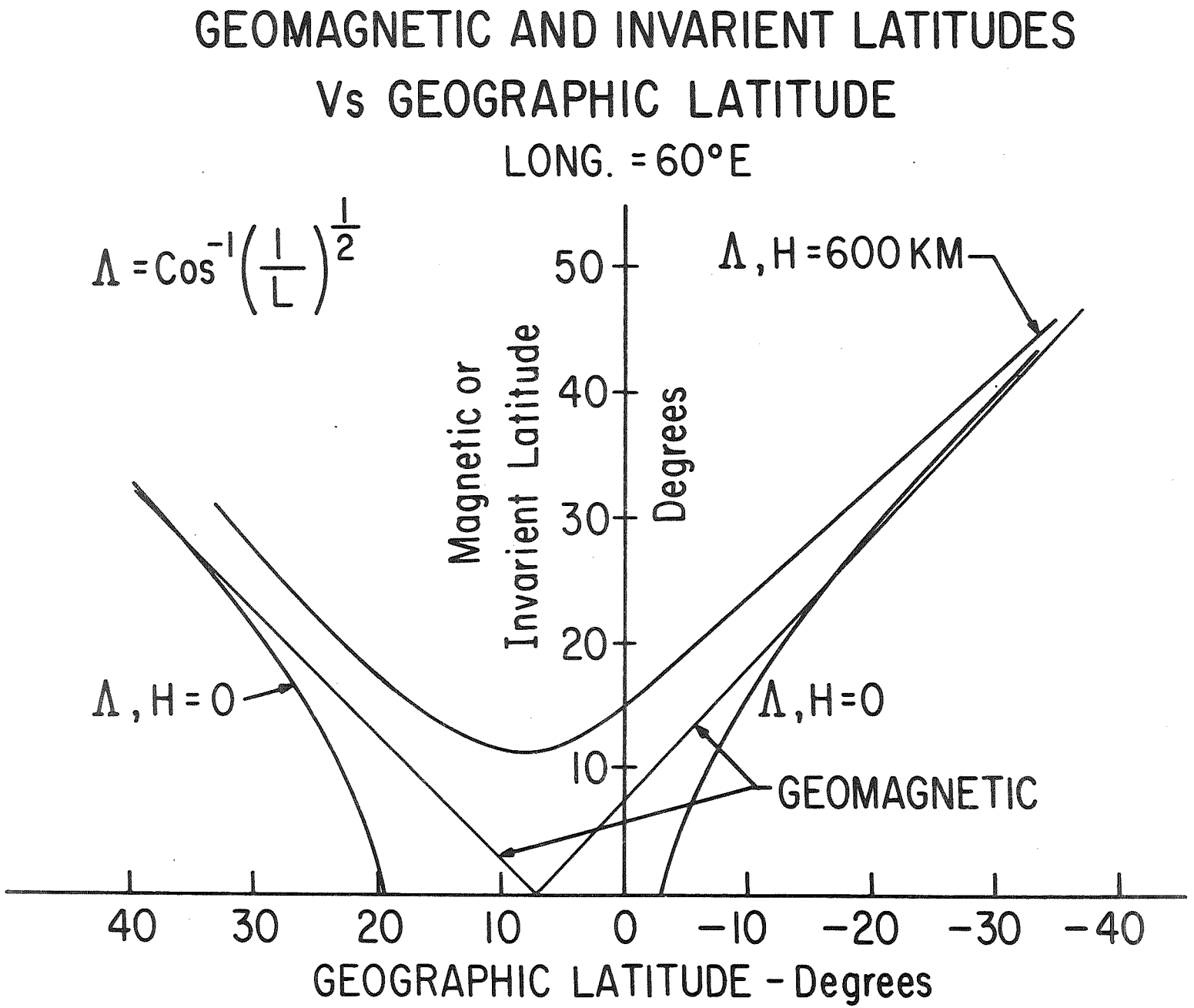
GEOMAGNETIC AND INVARIENT LATITUDES
Vs GEOGRAPHIC LATITUDE
LONG. = 60°E
$\Lambda = \cos^{-1}\left(\frac{1}{L}\right)^{\frac{1}{2}}$
Λ, H = 600 KM
Λ, H = 0
Λ, H = 0
GEOMAGNETIC
Magnetic or Invarient Latitude Degrees
50
40
30
20
10
40 30 20 10 0 −10 −20 −30 −40
GEOGRAPHIC LATITUDE - Degrees

Figure 9

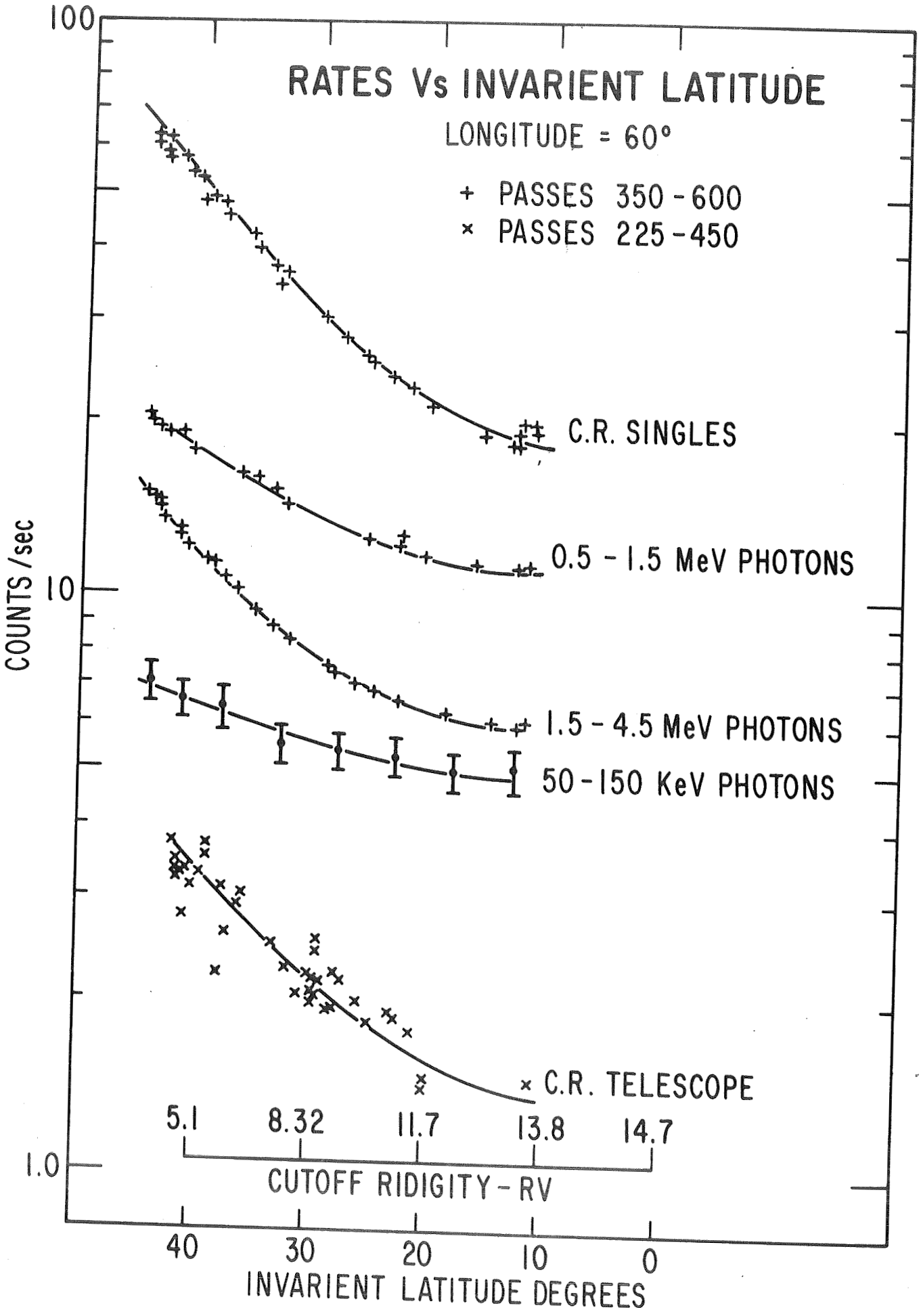
RATES Vs INVARIENT LATITUDE
LONGITUDE = 60°
+ PASSES 350 - 600
× PASSES 225 - 450
C.R. SINGLES
0.5 - 1.5 MeV PHOTONS
1.5 - 4.5 MeV PHOTONS
50 - 150 KeV PHOTONS
C.R. TELESCOPE
COUNTS / sec
100
10
1.0
5.1
8.32
11.7
13.8
14.7
CUTOFF RIDIGITY - RV
40
30
20
10
0
INVARIENT LATITUDE DEGREES

Figure 10

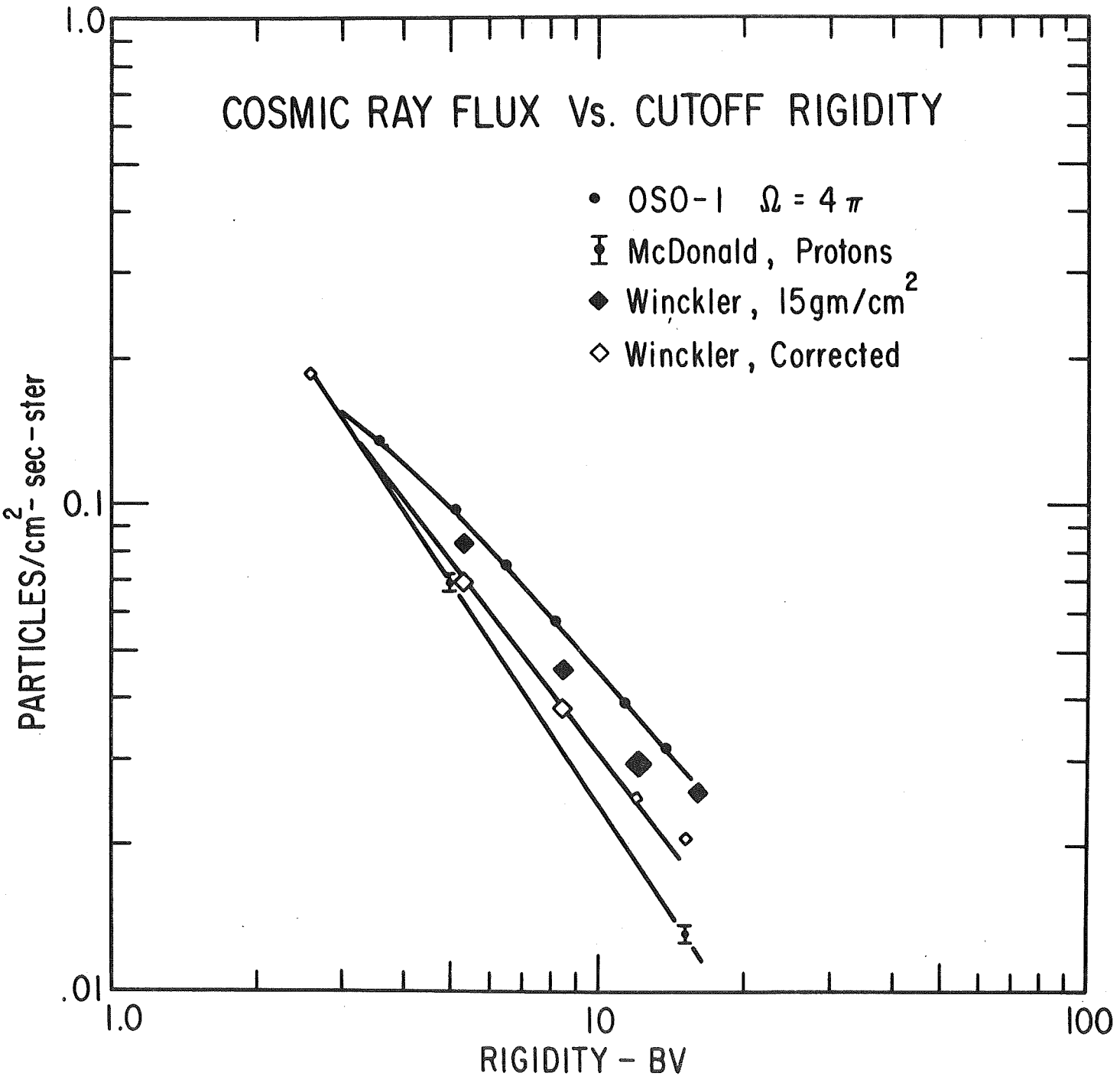
COSMIC RAY FLUX Vs. CUTOFF RIGIDITY
OSO-I Ω = 4π
McDonald, Protons
Winckler, 15gm/cm²
Winckler, Corrected
PARTICLES/cm²-sec-ster
1.0
0.1
.01
1.0
10
100
RIGIDITY - BV

Figure 11

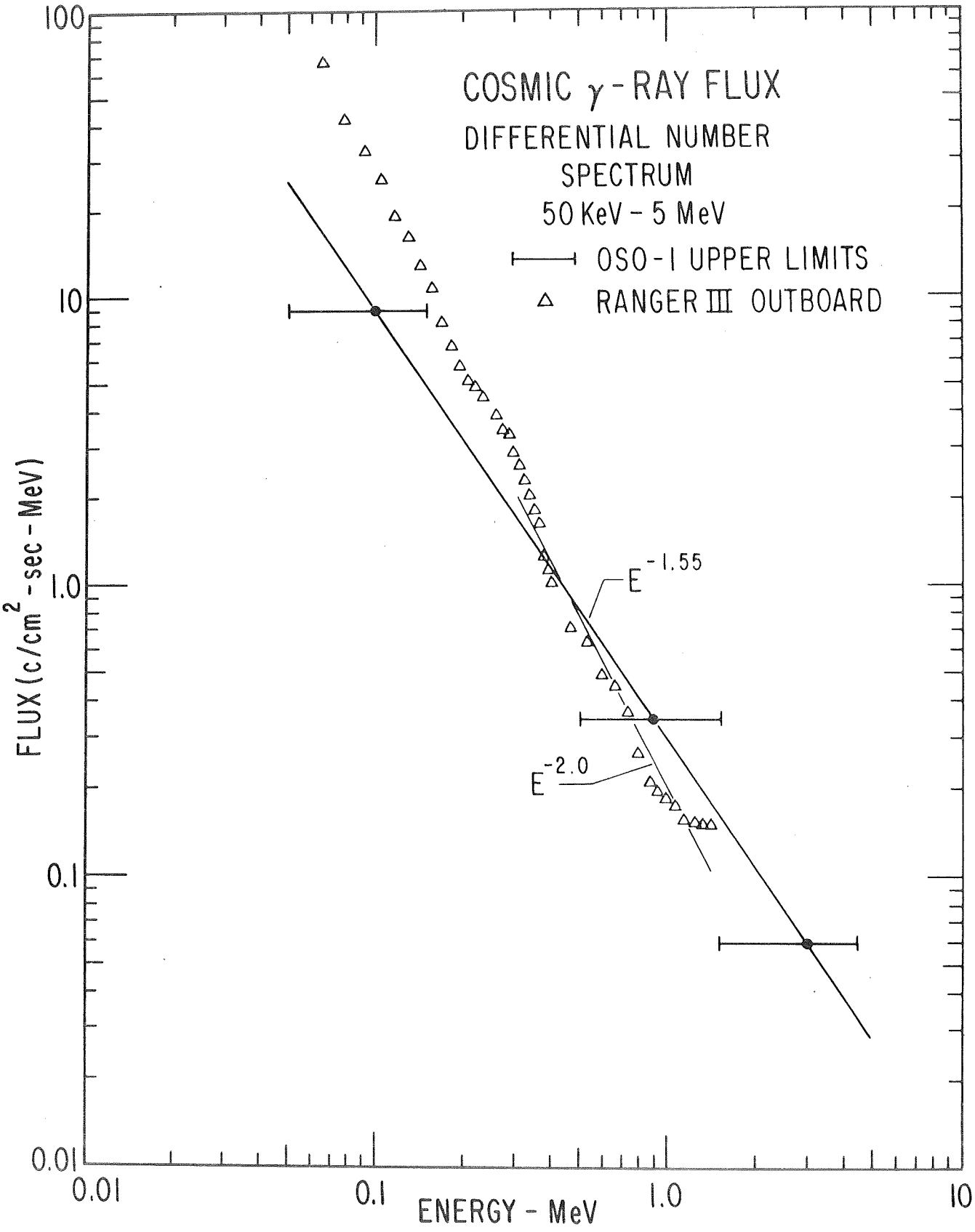
COSMIC γ - RAY FLUX
DIFFERENTIAL NUMBER
SPECTRUM
50 KeV - 5 MeV
OSO - I UPPER LIMITS
RANGER III OUTBOARD
E^-1.55
E^-2.0
FLUX (c/cm^2 - sec - MeV)
ENERGY - MeV
100
10
1.0
0.1
0.01
0.01
0.1
1.0
10

Figure 12

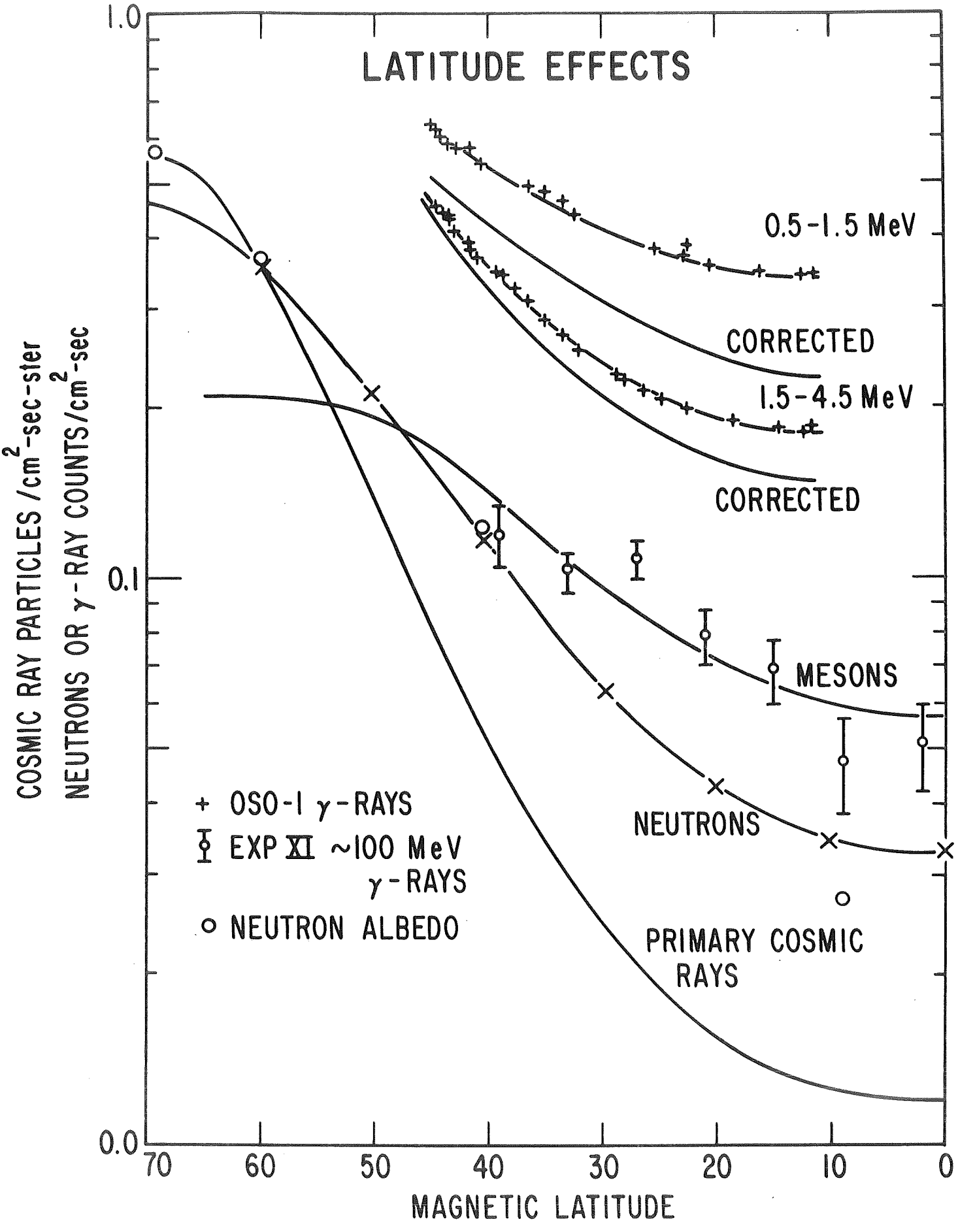
LATITUDE EFFECTS
1.0
0.1
0.0
0.5-1.5 MeV
CORRECTED
1.5-4.5 MeV
CORRECTED
MESONS
NEUTRONS
PRIMARY COSMIC RAYS
+ OSO-I γ-RAYS
EXP XI ~100 MeV γ-RAYS
NEUTRON ALBEDO
COSMIC RAY PARTICLES /cm²-sec-ster
NEUTRONS OR γ-RAY COUNTS/cm²-sec
70
60
50
40
30
20
10
0
MAGNETIC LATITUDE

Figure 13

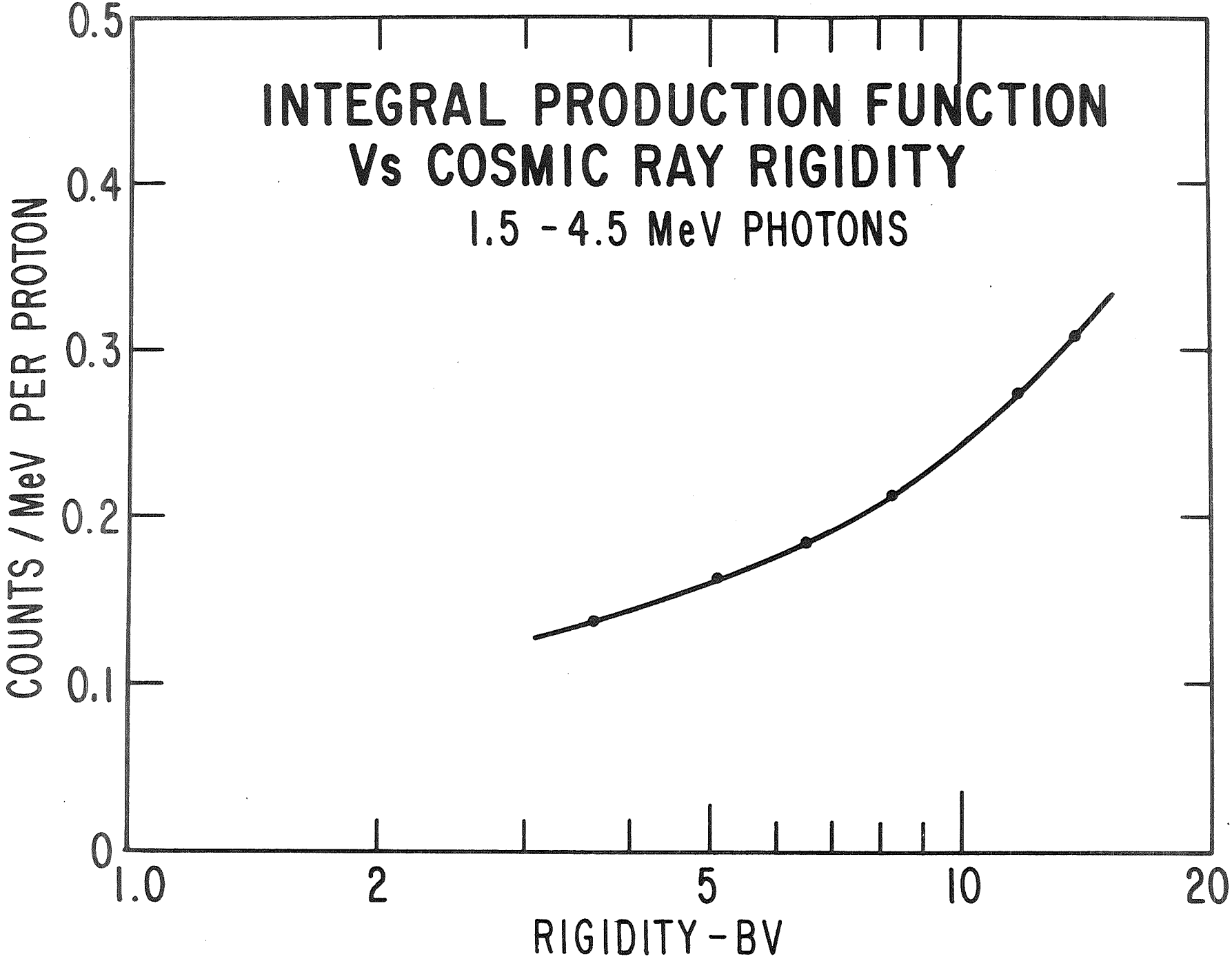
INTEGRAL PRODUCTION FUNCTION
Vs COSMIC RAY RIGIDITY
1.5 - 4.5 MeV PHOTONS
COUNTS / MeV PER PROTON
0.5
0.4
0.3
0.2
0.1
0
1.0
2
5
10
20
RIGIDITY - BV

Figure 14

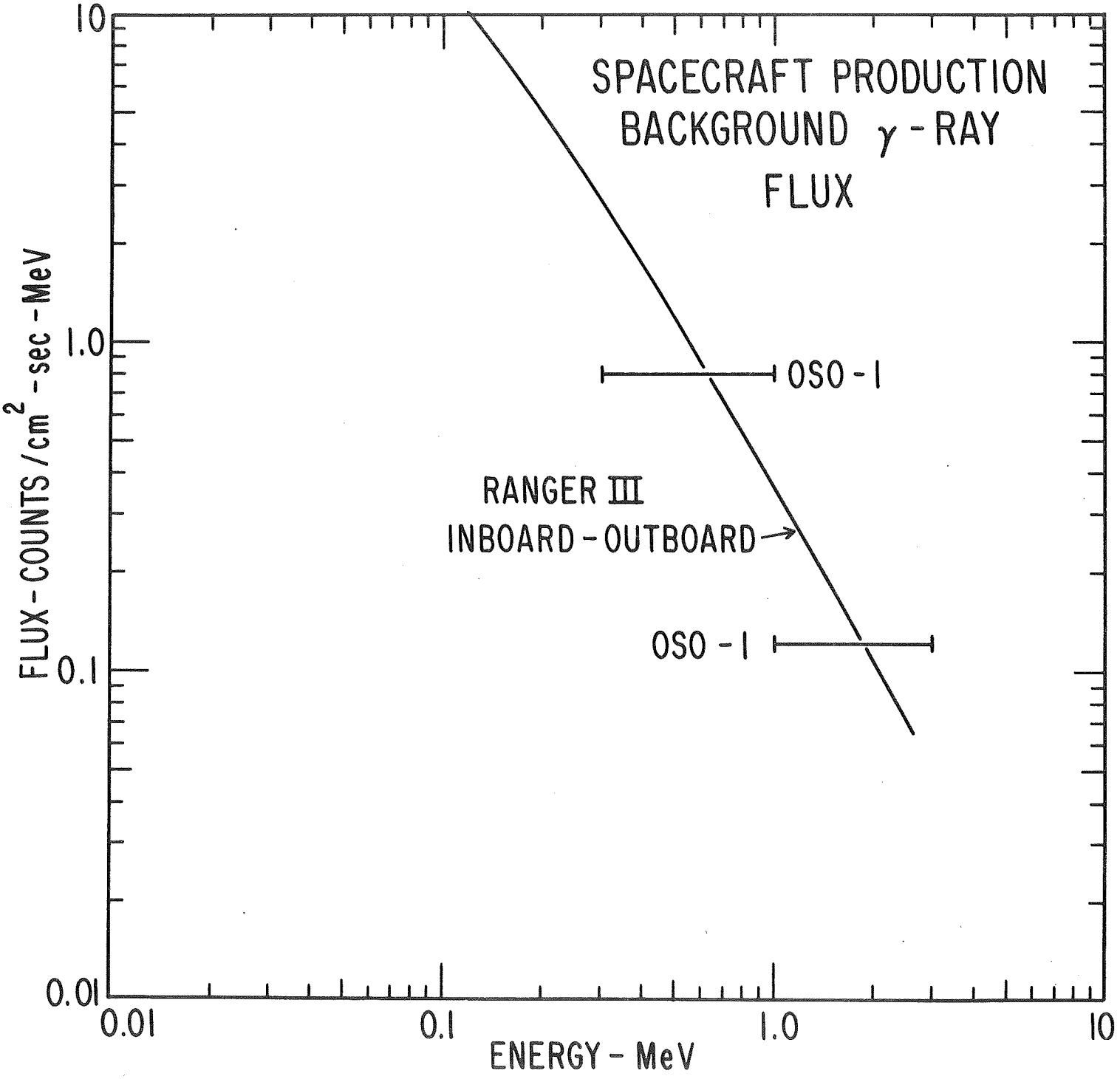
SPACECRAFT PRODUCTION
BACKGROUND γ - RAY
FLUX
OSO - I
RANGER III
INBOARD - OUTBOARD
OSO - I
FLUX - COUNTS / cm² - sec - MeV
ENERGY - MeV
10
1.0
0.1
0.01
0.01
0.1
1.0
10

Figure 15